JCB Journal of Cell Biology

ARTICLE

Microglial TNFα controls daily changes in synaptic $GABA_A$Rs and sleep slow waves

Maria Joana Pinto[1], Lucy Bizien[1], Julie M.J. Fabre[1], Nina Đukanović[1], Valentin Lepetz[1], Fiona Henderson[2], Marine Pujol[2], Romain W. Sala[1], Thibault Tarpin[1], Daniela Popa[1], Antoine Triller[1], Clément Léna[1], Véronique Fabre[2], and Alain Bessis[1]

Microglia sense the changes in their environment. How microglia actively translate these changes into suitable cues to adapt brain physiology is unknown. We reveal an activity-dependent regulation of cortical inhibitory synapses by microglia, driven by purinergic signaling acting on P2RX7 and mediated by microglia-derived TNFα. We demonstrate that sleep induces microglia-dependent synaptic enrichment of $GABA_A$Rs in a manner dependent on microglial TNFα and P2RX7. We further show that microglia-specific depletion of TNFα alters slow waves during NREM sleep and blunt memory consolidation in sleep-dependent learning tasks. Together, our results reveal that microglia orchestrate sleep-intrinsic plasticity of synaptic $GABA_A$Rs, sculpt sleep slow waves, and support memory consolidation.

Introduction

Microglia, the immune cells of the brain, tune neuronal networks in the healthy brain by finely modulating synapses (Kettenmann et al., 2013). They can sculpt developing circuits and remodel neuronal connectivity in adulthood by adjusting synapse density, function, and plasticity (Favuzzi et al., 2021; Nguyen et al., 2020; Parkhurst et al., 2013; Schafer et al., 2012; Wang et al., 2020). Microglia accomplish these functions either by direct interaction with synaptic elements (Miyamoto et al., 2016a; Schafer et al., 2012) or through the release of factors (Lewitus et al., 2016; Parkhurst et al., 2013). Many of the latter, such as prostaglandin, BDNF, IL-1β, or TNFα, control synaptic plasticity and were independently shown to regulate sleep (Porkka-Heiskanen, 2013). Recent work highlights the ability of microglia to control sleep duration (Corsi et al., 2022; Liu et al., 2021); however, whether and how microglia-released factors shape sleep remains unclear.

TNFα not only regulates synaptic strength by supporting glutamatergic gliotransmission (Santello et al., 2011) but also controls the homeostasis of synaptic strength during synaptic scaling by adapting synaptic trafficking of AMPARs (Stellwagen and Malenka, 2006; Beattie et al., 2002). The role of TNFα in sleep was demonstrated by the administration of exogenous TNFα which promotes non-rapid eye movement (NREM) sleep (Fang et al., 1997; Yoshida et al., 2004) whereas inhibition of endogenous TNFα reduces NREM sleep (refs in Rockstrom et al., 2018). Similarly, intracerebral or intraperitoneal injection of TNFα (Shoham et al., 1987) suppresses rapid eye movement (REM) sleep, which is increased in TNFα KO mice (Szentirmai and Kapás, 2019). Of note, transcriptomic analysis showed a near-exclusive expression of TNFα by microglia in the brain (Zamanian et al., 2012; Zeisel et al., 2018). Nevertheless, it remains unclear whether microglial TNFα is involved in sleep-associated synaptic plasticity and sleep regulation.

Sleep drives the plasticity of excitatory synapses. In the cortex, spine turnover during sleep is associated with learning and memory (Yang et al., 2014; Li et al., 2017) and, in parallel, wake-associated strengthening of excitatory synapses is downscaled during sleep (Diering et al., 2017; Vyazovskiy et al., 2008). These studies only focus on excitatory synapses, and the regulation of inhibitory synapses during sleep has barely been studied (Bridi et al., 2020). The likely, yet unknown, contribution of inhibitory plasticity is highlighted by the fact that cortical GABAergic inhibition regulates sleep oscillations including slow waves (Funk et al., 2017; Niethard et al., 2018) and that modulators of $GABA_A$Rs are commonly used as sleeping pills (Dixon et al., 2015). Here, we uncover the molecular pathway underlying sleep-intrinsic microglia-dependent modulation of synaptic $GABA_A$R in light versus dark periods. We then demonstrate that microglial TNFα shapes sleep slow waves and supports memory consolidation.

[1]Institut de Biologie de l'École Normale Supérieure (IBENS), École Normale Supérieure, CNRS, INSERM, Université PSL, Paris, France; [2]Neurosciences Paris Seine—Institut de Biologie Paris Seine (NPS—IBPS), CNRS, INSERM, Sorbonne Universités, Paris, France.

Correspondence to Alain Bessis: alain.bessis@bio.ens.psl.eu; Clément Léna: clement.lena@bio.ens.psl.eu; Véronique Fabre: veronique.fabre@inserm.fr.

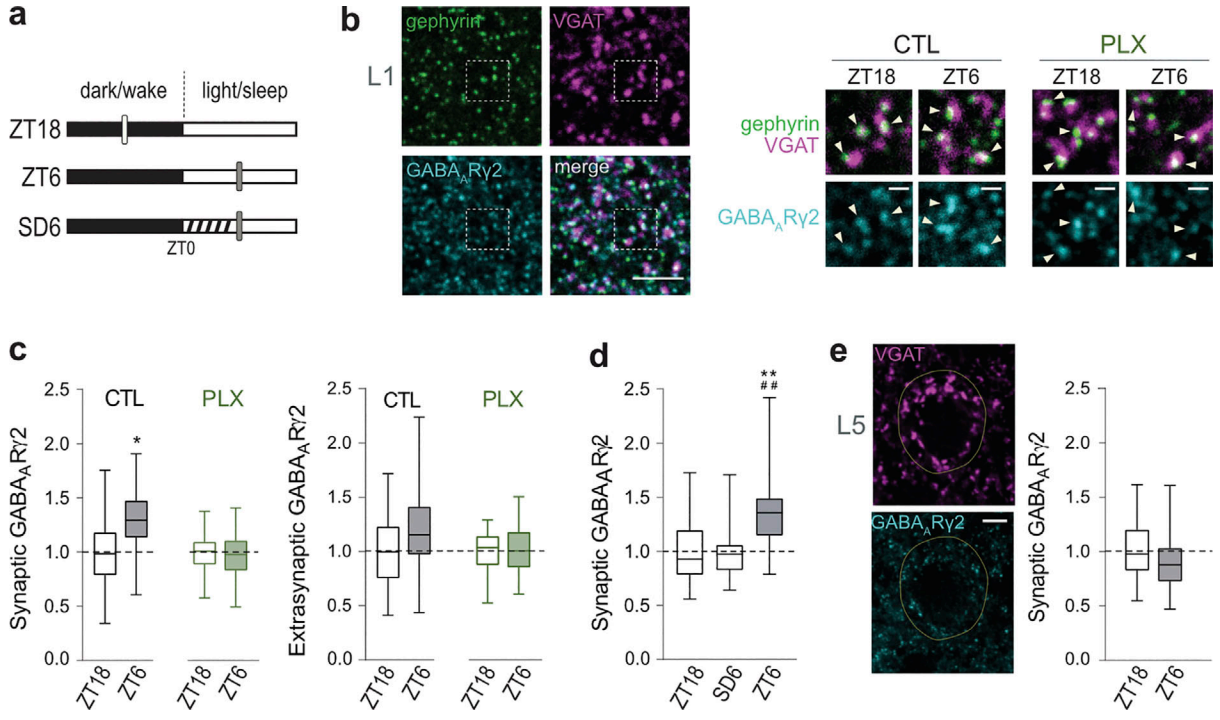

Figure 1. **Plasticity of GABA$_A$R in light versus dark is sleep- and microglia-dependent. (a)** Experimental groups: mice in dark phase (ZT18), mice in light phase (ZT6), and mice submitted to sleep deprivation (dashed) in the light phase (SD6). Vertical bars: time of perfusion. **(b)** Representative images showing enrichment of GABA$_A$Rγ2 (cyan) at cortical L1 inhibitory synapses in the light phase (ZT6). Arrowheads: GABA$_A$Rγ2 clusters at gephyrin$^+$VGAT$^+$ synapses in control (CTL) or PLX3397-treated mice (PLX). Scale bars, 5 and 1 µm. The dashed box corresponds to CTL at ZT18. **(c and d)** Mean intensity of GABA$_A$Rγ2 clusters at gephyrin$^+$VGAT$^+$ synapses (synaptic) and at extrasynaptic sites normalized to ZT18. *n* = 48–65 fields of view (FOVs) from 4 to 5 mice per group. *P < 0.05, nested two-tailed *t* test; **P < 0.01 compared with ZT18 and ##P < 0.01 compared with SD6, nested one-way ANOVA followed by Sidak's multiple comparison test. **(e)** Left: Representative confocal images of VGAT and GABA$_A$Rγ2 in cortical L5. Yellow line delineates soma identified by NeuN staining. Scale bar, 5 µm. Right: Mean intensity of GABA$_A$Rγ2 at somatic VGAT$^+$ clusters in L5 normalized to ZT18. *n* = 60 FOVs from five mice per group. No statistical significance by nested two-tailed *t* test. **(c–e)** Results are presented as minimum to maximum box plots.

Results

Daily modulation of GABA$_A$Rs in a sleep- and microglia-dependent manner

We first analyzed the modulation of synapses in the frontal cortex in light versus dark by measuring the synaptic content of neurotransmitter receptors (Figs. 1, S1, and S2). Mice sleep more during the light phase and spend most of the dark phase awake. Therefore, we compared the brains of mice at Zeitgeber time 18 (ZT18; dark/middle of wake phase) and at ZT6 (light/middle of sleep phase; Fig. 1 a). We focused on cortical layer 1 (L1) which is a key node for wide-scale cortical computation (Schuman et al., 2021). Consistent with the well-established downscaling of excitatory synapses during sleep (Diering et al., 2017), synaptic accumulation of the AMPA receptor subunit GluA2 was modestly but significantly decreased at ZT6 as compared with ZT18 (Fig. S1). Of note, this level of change is comparable with previous analysis of daily changes in synaptic AMPARs (Diering et al., 2017; Noya et al., 2019). Yet, analysis of L1 inhibitory synapses revealed an increased enrichment of synaptic, but not extra-synaptic, GABA$_A$R-γ2 and -α1 subunits at ZT6 (Fig. 1, a–c and Fig. S2, b–d), as well as an enhanced proportion of inhibitory synapses containing a GABA$_A$R cluster (Fig. S2 e). No changes were observed in the total signal of GABA$_A$Rs (Fig. S2 g), supportive of redistribution of the receptors rather than changes in expression. In contrast, in layer 5 (L5), the synaptic content of GABA$_A$Rγ2 did not significantly differ between ZT6 and ZT18 (Fig. 1 e and Fig. S2 f). These results reveal a novel form of regulation of GABAergic synapses in light versus dark periods with synaptic enrichment of GABA$_A$Rs in L1 during the light phase (ZT6), which likely contributes to the upregulation of inhibitory transmission in the upper cortex during this phase (Bridi et al., 2020).

To discriminate between a sleep-intrinsic or time-of-day-dependent regulation of synaptic GABA$_A$R in L1, mice were forced to stay awake during their normal sleep period (sleep deprivation from ZT0 to ZT6, SD6; Fig. 1 a). The synaptic content of GABA$_A$R was not different between mice at ZT18 and mice sleep-deprived in the light phase (SD6; Fig. 1 d), showing that modulation of synaptic GABA$_A$R in L1 is driven by sleep-dependent mechanisms. Sleep deprivation has previously been shown to increase GABA$_A$Rs located around excitatory somas at cortical layers 2–6 (Del Cid-Pellitero et al., 2017). In our study, we focused on cortical L1, where most of the inhibitory synapses are dendritic (Tremblay et al., 2016). Together, this suggests that the expression of GABA$_A$Rs is differentially regulated by sleep depending on their subcellular localization.

We have previously shown that microglia control the accumulation of receptors at inhibitory synapses in the spinal cord

(Cantaut-Belarif et al., 2017). This prompted us to investigate the involvement of microglia in the modulation of synaptic $GABA_AR$ in light versus dark periods. Strikingly, microglia depletion by feeding mice with the CSF1R antagonist PLX3397 (Elmore et al., 2014) (PLX; Fig. S2, a and b) completely prevented the changes in synaptic $GABA_ARs$ content between ZT6 and ZT18 (Fig. 1 c and Fig. S2, b and e). Importantly, as already shown (Corsi et al., 2022; Liu et al., 2021), microglia depletion does not alter sleep during the light phase (Fig. S2, h and i; and Table S1), discarding the possibility that lack of synaptic $GABA_ARs$ enrichment upon PLX3397 treatment results from perturbed sleep during the light phase. This shows that the sleep-dependent modulation of synaptic $GABA_AR$ in L1 requires microglia. Moreover, microglia depletion also reversed the reduction of synaptic AMPA receptor subunit GluA2 at ZT6 (Fig. S1), which agrees with the recent demonstration that light/dark changes in excitatory synaptic strength are microglia-dependent (Corsi et al., 2022), a function that has been attributed to CX3CR1 signaling (Corsi et al., 2022) and that was not further explored in this study.

Modulation of synaptic $GABA_AR$ by microglial P2RX7-TNFα signaling via CaMKII

We next sought to identify the molecular pathway underlying this novel microglia-dependent synaptic regulation. To accomplish so, we identified the molecular candidates regulating synaptic $GABA_ARs$ enrichment in an ex vivo paradigm of plasticity (Fig. 2) and subsequently validated these candidates in vivo (Fig. 3). During sleep, excitatory synaptic plasticity is triggered by NMDAR-dependent dendritic calcium spikes in L1 (Li et al., 2017). We thus selected an NMDA-induced GABAergic plasticity protocol, known as inhibitory long-term potentiation (iLTP). This form of plasticity, known to drive depression of excitatory synapses (Lee et al., 1998), also leads to upregulation of synaptic $GABA_ARs$ (Petrini et al., 2014) in pyramidal neurons specifically at somatostatin interneurons inputs (SOM-IN) (Chiu et al., 2018), which are mainly located in L1 (Tremblay et al., 2016) (Fig. S3). In agreement with the SOM-IN topographical organization, NMDA-induced iLTP in brain organotypic slices led to specific synaptic enrichment of $GABA_ARs$ in L1 but not in L5 somatic synapses (Fig. 2, a and b; and Fig. S4, b–d). This protocol thus mimics ex-vivo the synaptic regulations occurring in light versus dark, and we used it to identify the actors of the L1-restricted sleep-dependent synaptic enrichment of $GABA_ARs$ (Fig. 1). We further demonstrated that this form of $GABA_AR$ plasticity was completely abolished when microglia were depleted by PLX (Fig. 2, a and b; and Fig. S4, a and c). We ruled out possible secondary effects of PLX by showing the same effect upon microglia depletion using Mac1-Saporin (SAP) (Fig. S4 a) or inactivation using minocycline (Fig. 2 b).

Microglia produce a broad repertoire of signaling molecules that regulate synaptic function (Kettenmann et al., 2013). TNFα, which is mostly if not exclusively produced by microglia in the brain (Zeisel et al., 2018), controls basal synaptic strength (Santello et al., 2011), neurotransmitter receptors' dynamics, and homeostatic synaptic plasticity (Stellwagen and Malenka, 2006). We thus hypothesized that microglial TNFα controls the activity-dependent regulation of synaptic $GABA_AR$. Indeed, neutralization of TNFα by specific antibodies (Fig. 2 c) as well as conditional microglia-specific TNFα depletion (Fig. 2 d and Fig. S5 a) prevented the enrichment of synaptic $GABA_AR$ upon iLTP. Soluble TNFα derives from the cleavage of a membrane form of TNFα by the TNFα-converting enzyme (TACE) (Black et al., 1997). Both forms can signal through TNFR1, whereas TNFR2 is only activated by membrane TNFα (Holbrook et al., 2019). The increase of synaptic $GABA_ARs$ on iLTP-treated slices was prevented by TAPI-1, a TACE inhibitor, and by a TNFR1- but not by a TNFR2-neutralizing antibody (Fig. S5 b). Finally, we showed that recombinant TNFα and activation of TNFR1 were sufficient to increase synaptic accumulation of $GABA_AR\alpha1$ (Fig. S5, c–f). These experiments show that microglial soluble TNFα acting through TNFR1 mediates the activity-dependent regulation of $GABA_ARs$ in L1.

We next identified the signaling pathway between neurons and microglia leading to TNFα release upstream of $GABA_ARs$ regulation. We first demonstrated that the well-established neuronal CX_3CL1-microglial CX_3CR1 signaling, with known roles in synaptic plasticity (Rogers et al., 2011), is not involved (Fig. S4 e). Microglia behavior is finely tuned by ATP via an array of purinergic receptors (Madry and Attwell, 2015). Microglial cells rapidly react to ATP following the activation of neurons by glutamate and NMDA (Li et al., 2012; Dissing-Olesen et al., 2014; Badimon et al., 2020), and the stimulation of microglial P2RX7 promotes the release of TNFα (Suzuki et al., 2004). We thus investigated whether NMDA-induced release of ATP causes microglia-mediated modulation of synaptic $GABA_AR$. Indeed, apyrase, a promoter of ATP hydrolysis, PPADS, a broad P2RX antagonist, or A740003, a specific P2RX7 antagonist, prevented the increase of synaptic $GABA_AR$ upon iLTP. In contrast, PSB0739, a specific inhibitor of P2RY12 (Hoffmann et al., 2009), had no effect on synaptic $GABA_AR$ upon iLTP, suggesting that P2RY12 is not involved in this regulation (Fig. 2 e). Moreover, BzATP, a P2RX7 agonist (Surprenant et al., 1996), was sufficient to increase postsynaptic $GABA_AR\alpha1$ in L1 (Fig. 2 f; and Fig. S6, a and b) but not in L5 (Fig. S6 c). Of note, BzATP had no effect when microglia were depleted or when TNFα was specifically inactivated in microglia (Fig. 2 f). Thus, ATP/P2RX7 signaling acts upstream of microglial TNFα release to modulate synaptic accumulation of $GABA_AR$.

Finally, we explored the intracellular signaling downstream of microglial TNFα. CaMKIIα is a central neuronal mediator of postsynaptic plasticity whose activity is triggered by Ca^{2+}/calmodulin and can be prolonged in a Ca^{2+}-independent manner by its autophosphorylation at Thr286 (Bayer and Schulman, 2019). Upon iLTP, Thr286-autophosphorylated CaMKIIα leads to the insertion of $GABA_ARs$ at synapses (Marsden et al., 2010). We reasoned that TNFα may modulate CaMKIIα Thr286-phosphorylation, as observed in non-neuronal cells (Defer et al., 2007). Indeed, Thr286-phosphorylation of CaMKII was increased in L1 upon iLTP (Fig. 2 g), and this increase was abolished by microglial depletion and by blocking P2RX7 or TNFα signaling (Fig. 2 h). In agreement, BzATP, which upregulates the synaptic content of $GABA_ARs$ via a microglial relay, was sufficient to enhance CaMKII Thr286-phosphorylation (Fig. 2, g and h). The finding that CaMKII Thr286 phosphorylation,

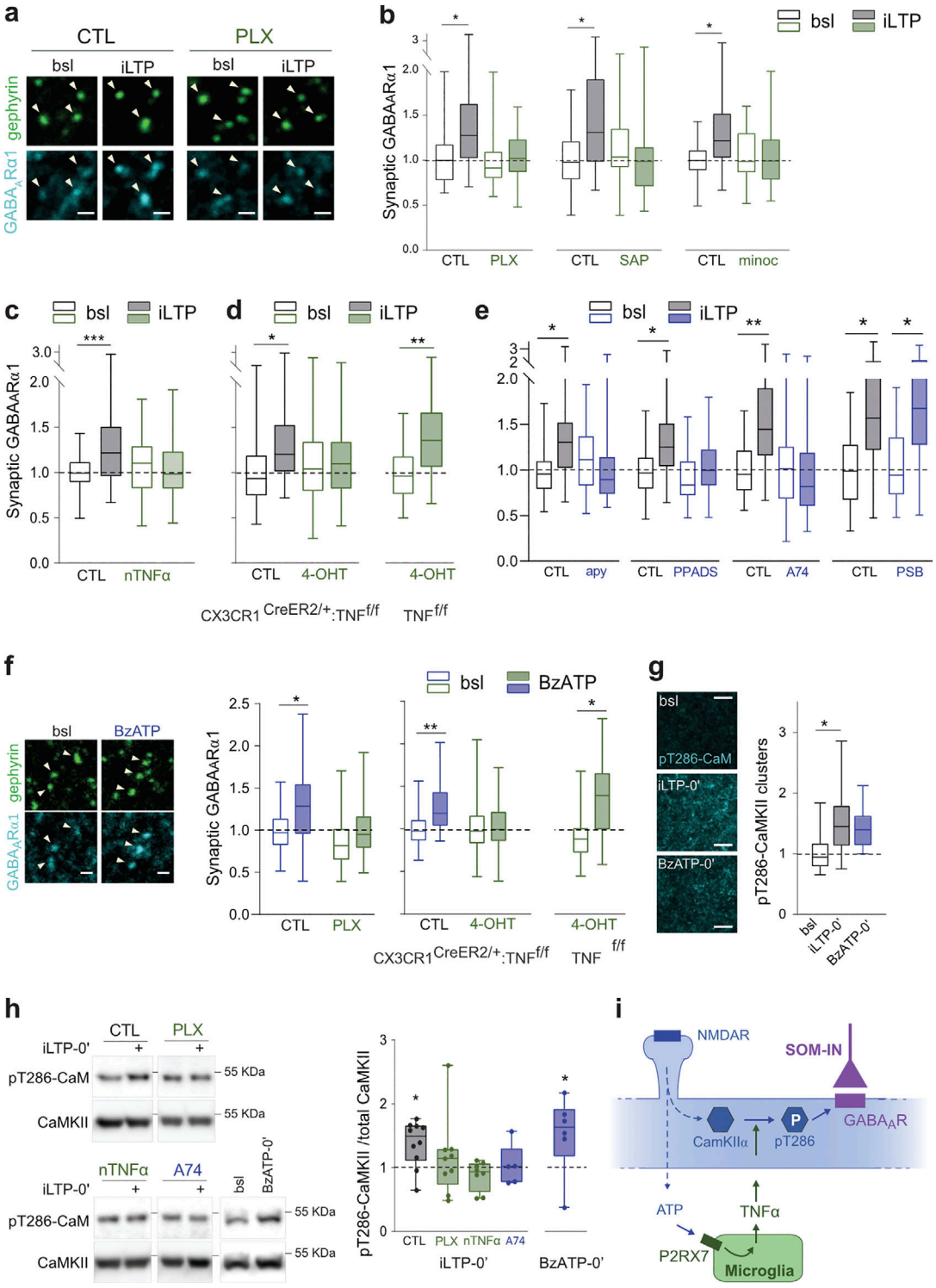

Figure 2. **Microglial P2RX7-TNFα signaling drives GABA$_A$Rs synaptic enrichment through CaMKIIα phosphorylation. (a)** Representative confocal images showing increase of GABA$_A$Rα1 (cyan) at gephyrin$^+$ clusters (arrowheads) upon NMDA-induced inhibitory long-term potentiation (iLTP: 2 min 20 µM NMDA/10 µM CNQX plus 20 min recovery) in organotypic slices cortical L1 (CTL: control; bsl: baseline). Scale bars, 1 µm. **(b–e)** Mean intensity of GABA$_A$Rα1 clusters at gephyrin$^+$ cluster normalized to CTL at bsl. *n* = FOVs/independent experiments: (b) *n* = 44–69/5–6; (c) *n* = 47–53/5; (d) *n* = 66–102/5–7; (e) *n* = 49–68/7–9. *P < 0.05, **P < 0.01 and ***P < 0.001, nested one-way ANOVA followed by Sidak's multiple comparison test. iLTP-induced synaptic GABA$_A$R enrichment is abolished by: b, microglia depletion/inactivation (PLX: PLX3397; SAP: Mac1-saporin; minoc: minocycline); c, neutralization of TNFα (nTNFα); d, microglia-specific TNFα deletion through 4-hydroxy-tamoxifen (4-OHT)-induced recombination on CX3CR1$^{CreER2/+}$:TNF$^{f/f}$ but not on a TNF$^{f/f}$ background; e, ATP hydrolysis (apy), P2RX antagonist (PPADS) and P2RX7 antagonist (A74), but not P2Y12R inhibitor (PSB). **(f)** Left: Confocal images of GABA$_A$Rα1 (cyan) at gephyrin$^+$ clusters (arrowheads) in bsl and upon BzATP treatment. Scale bars, 1 µm. Right: Mean intensity of GABA$_A$Rα1 clusters at gephyrin$^+$ clusters normalized to CTL at bsl. *n* = 49–63/5–6. *P < 0.05, **P < 0.01, nested one-way ANOVA followed by Sidak's multiple comparison test. **(g)** Left: Thr286-

phosphorylated CaMKII is enhanced in L1 at the induction phase of plasticity (iLTP0′ or BzATP0′). Scale bars, 5 µm. Right: Mean intensity of Thr286-phosphorylated CaMKII puncta normalized to bsl. *n* = 25 to 33 FOVs from three independent experiments. *P < 0.05, one-way ANOVA followed by Sidak's multiple comparison test. **(h)** Left: Western blot analysis showing iLTP0′-induced CaMKII Thr286-phosphorylation. Right: Ratio between Thr286-phosphorylated CaMKII and total CaMKII normalized to the respective iLTP-free control. *n* = 5–9 independent experiments. *P < 0.05 compared with respective control, Kruskal–Wallis test followed by Dunn's multiple comparisons test. **(b–h)** Results are presented as minimum to maximum box plots. **(i)** Model. ATP released downstream NMDA-induced neuronal activity activates microglial P2RX7 which triggers the release of microglial TNFα. TNFα signaling gates CaMKIIα autophosphorylation which controls the enrichment of synaptic $GABA_A$Rs in pyramidal neurons. Source data are available for this figure: SourceData F2.

and therefore its activity, is gated by microglial TNFα downstream neuronal activity emphasizes a cardinal position of microglia in fine-tuning synapses.

Collectively, our results support a bidirectional neuron-microglia crosstalk underlying activity-driven GABAergic potentiation in L1 (Fig. 2 i): ATP released downstream neuronal activity activates microglial P2RX7 with concomitant release of TNFα which modulates CaMKII autophosphorylation and thereby enrichment of synaptic $GABA_A$Rs. Noteworthy, our results do not exclude the possible involvement of other cell types acting between neurons and microglia.

Sleep-dependent modulation of synaptic $GABA_A$R driven by P2RX7 and microglial TNFα

Having shown that the microglial P2RX7/TNFα pathway controls L1 activity-dependent $GABA_A$R plasticity via CaMKII autophosphorylation ex-vivo, we examined the involvement of this pathway in the sleep-dependent modulation of synaptic $GABA_A$R in light versus dark (Fig. 1). We first showed that CaMKII Thr286-phosphorylation, but not total CaMKII levels, was increased in L1 at ZT6 (Fig. 3, a and b). Notably, such regulation was not found in L5 (Fig. S7 b). Next, we showed that Thr286-phosphorylation of CaMKII, as well as the synaptic content of $GABA_A$Rs in L1, was not enhanced at ZT6 in mice with microglia-specific TNFα depletion (micTNFα-KO, Fig. S5 a) and in P2rx7-KO mice (Fig. 3, a–c; and Fig. S7, c and d). Importantly, loss of enhancement at ZT6 is likely not attributed to disturbed sleep since deletion of P2RX7 (Krueger et al., 2010) or deletion of microglial TNFα (as discussed in the next section, Fig. 4) do not cause major changes in baseline sleep (Table S2). This shows that P2RX7 and microglial TNFα are required for daily fluctuations of CaMKII Thr286-phosphorylation and synaptic $GABA_A$R in cortical L1, which occur in a manner dependent on sleep in the light phase.

NREM slow waves shaped by microglial TNFα

The results above show that microglial TNFα is required for a novel sleep-dependent regulation of inhibitory synapses in cortical L1. TNFα is an established sleep factor; however, the contribution of microglial TNFα to physiological sleep remains unknown. Sleep is an alternation of REM and NREM sleep periods, which are hallmarked by major EEG oscillatory patterns (Adamantidis et al., 2019). During NREM sleep, slow waves in the delta frequency band (0.1–4 Hz), quantified as slow wave activity (SWA), result from the synchronous alternation of active (up) and silent (down) states of cortical neurons. Cortical GABAergic inhibition is a major actor of NREM sleep slow waves (Hay et al., 2021; Lemieux et al., 2015). We thus set out to explore the contribution of microglial TNFα in regulating sleep and shaping SWA. Sleep was analyzed using EMG and epidural EEG recordings, and we concentrated our analysis in the frontal cortex, where slow waves are predominant (Vyazovskiy et al., 2006). We first showed that microglial TNFα has limited effects on sleep–wake patterns as shown by the lack of major alterations in the amounts of wake, NREM, and REM sleep between micTNFα-KO and tCTL mice along a light/dark cycle (Fig. 4 a).

We then analyzed the spectral density of the EEG during sleep (Fig. 4 b). In agreement with a role of microglial TNFα in the regulation of SWA, we found a shift in the EEG spectral density toward lower frequency activity during NREM sleep

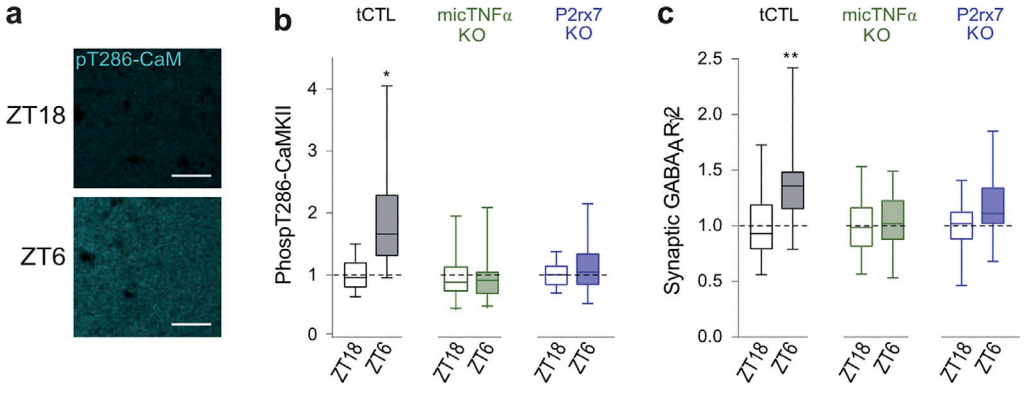

Figure 3. **P2RX7 and microglial TNFα promote daily changes in synaptic $GABA_A$R content and CaMKII phosphorylation. (a)** Representative confocal images of Thr286-phosphorylated CaMKII immunoreactivity in L1 show higher intensity at ZT6 than ZT18 in transgenic control mice (tCTL). Scale bars, 20 µm. **(b)** Mean intensity of Thr286-phosphorylated CaMKII signal in L1 normalized to ZT18 for tCTL, microglia-specific TNFα depletion (micTNFα-KO) and P2rx7-KO mice. *n* = 37–50 FOVs from four to five mice per group. **(c)** Mean intensity of $GABA_A$Rγ2 clusters at gephyrin$^+$VGAT$^+$ synapses normalized to ZT18. *n* = 48 to 65 FOVs from four to five mice per group. **(b and c)** *P < 0.05 and **P < 0.01, nested two-tailed t-test. Results are presented as minimum to maximum box plots.

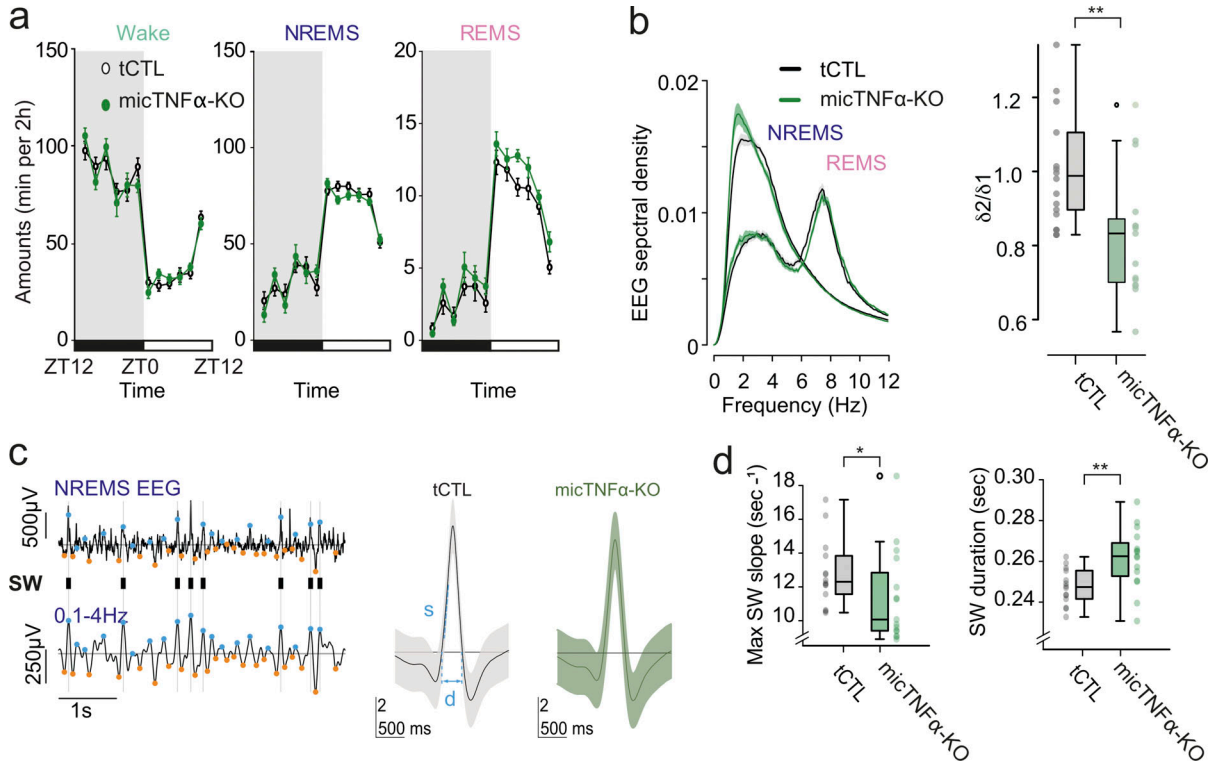

Figure 4. **Microglial TNFα modulates slow waves during NREMS. (a)** Amounts of vigilance states over 24 h reported by 2-h segments. Wake, NREMS, and REMS are not significantly different between tCTL and micTNFα-KO mice (n = 15 mice per group; two-way RM-ANOVA, P = 0.1490; P = 0.2784, P = 0.6838 respectively). **(b)** Left: Average spectral density (top) of tCTL and micTNFα-KO (lines: means; shaded area: SEM). Right: Ratio between power in faster delta frequencies (δ2, waves from 2.5 to 3.5 Hz) and slower delta frequencies (δ1, waves from 0.75 to 1.75 Hz) in NREM sleep (Mann-Whitney W = 169, P = 0.0043). **(c)** Left: Examples of EEG and 0.1–4 Hz filtered EEG during NREMS from a transgenic control tCTL; the positive and negative peaks of the delta-filtered signal are indicated by orange and blue points, respectively. Ticks on gray lines indicate large positive deflections corresponding to slow waves (SW). Right: Grand average SW for tCTL (black) showing duration (d) and maximum slope (s), and micTNFα-KO (green). **(d)** Characteristics of SW in a 24-h time period. micTNFα-KO mice exhibit significantly shorter peak onset slopes and longer SW duration than tCTL mice. Mann–Whitney W = 42 P = 0.005 and W = 153, P = 0.37 respectively. n = 14 tCTL and 15 micTNFα-KO respectively. **(b** [right] and **d)** Results are presented as minimum to maximum boxplots with the individual values of each mouse represented as datapoints.

with a slower peak frequency in the delta range in micTNFα-KO as compared with tCTL with no change in the delta power (Wilcoxon test: W = 67, P = 0.06) (Fig. 4 b). More precisely, a significant difference between the fraction of total EEG spectral density in the δ1 band (waves from 0.75 to 1.75 Hz; tCTL: 0.123 ± 0.004, micTNFα-KO: 0.148 ± 0.008; mean ± SEM; Wilcox statistics = 48, P value = 0.0120), but not in the δ2 band (2.5–3.5 Hz; tCTL: 0.122 ± 0.002, micTNFα-KO: 0.119 ± 0.003; mean ± SEM; Wilcox statistics = 122, P value = 0.4773) was observed in micTNFα-KO resulting in a decreased ratio of δ2 over δ1 power (Fig. 4 b right).

There were no detectable differences in the other frequency ranges nor in REM sleep (Fig. 4 b). Finally, we explored how microglial TNFα shapes the properties of individual slow waves during NREM sleep. Slow waves were identified in the epidural EEG as an alternation of large transient negative and positive deflections in the 0.1–4 Hz filtered EEG (Fig. 4 c). We verified that these deflections correspond to up and down states, respectively (Fig. S8) (Nir et al., 2011). Remarkably, the maximum ascending slope of the slow waves, which coincides with the onset of the cortical positive deflection (downstate; Fig. S8 c), was decreased (~17% decrease in micTNFα-KO as compared with tCTL, Fig. 4 d left), and the duration of the SW down state (Fig. S8, a and b) was increased in mice depleted of microglial TNFα as compared with controls (Fig. 4 d). These results indicate that microglial TNFα shapes slow waves during NREM sleep by favoring transition into the down states.

Microglial TNFα supports memory consolidation of specific learning tasks

Slow waves are known to play a causal role in the consolidation of memory during sleep (Fattinger et al., 2017; Marshall et al., 2006). To assess the role of microglial TNFα in the memory consolidation processes, we compared the consolidation of different learning tasks known to be sleep-dependent (Nagai et al., 2017; Miyamoto et al., 2016b; Rolls et al., 2011) in micTNFα-KO and tCTL mice. In a first learning paradigm (Nagai et al., 2017), mice learned to run on top of a complex wheel attached to an accelerating rotarod in a first 20-trial session (S1). After one day of ad libitum sleep, performance on the complex wheel was assessed on a second 20-trial session by measuring the latency to fall (S2; Fig. 5, a and b). We first confirmed that the learning, evaluated as the improvement of performance within each session, was not different between tCTL and micTNFα-KO

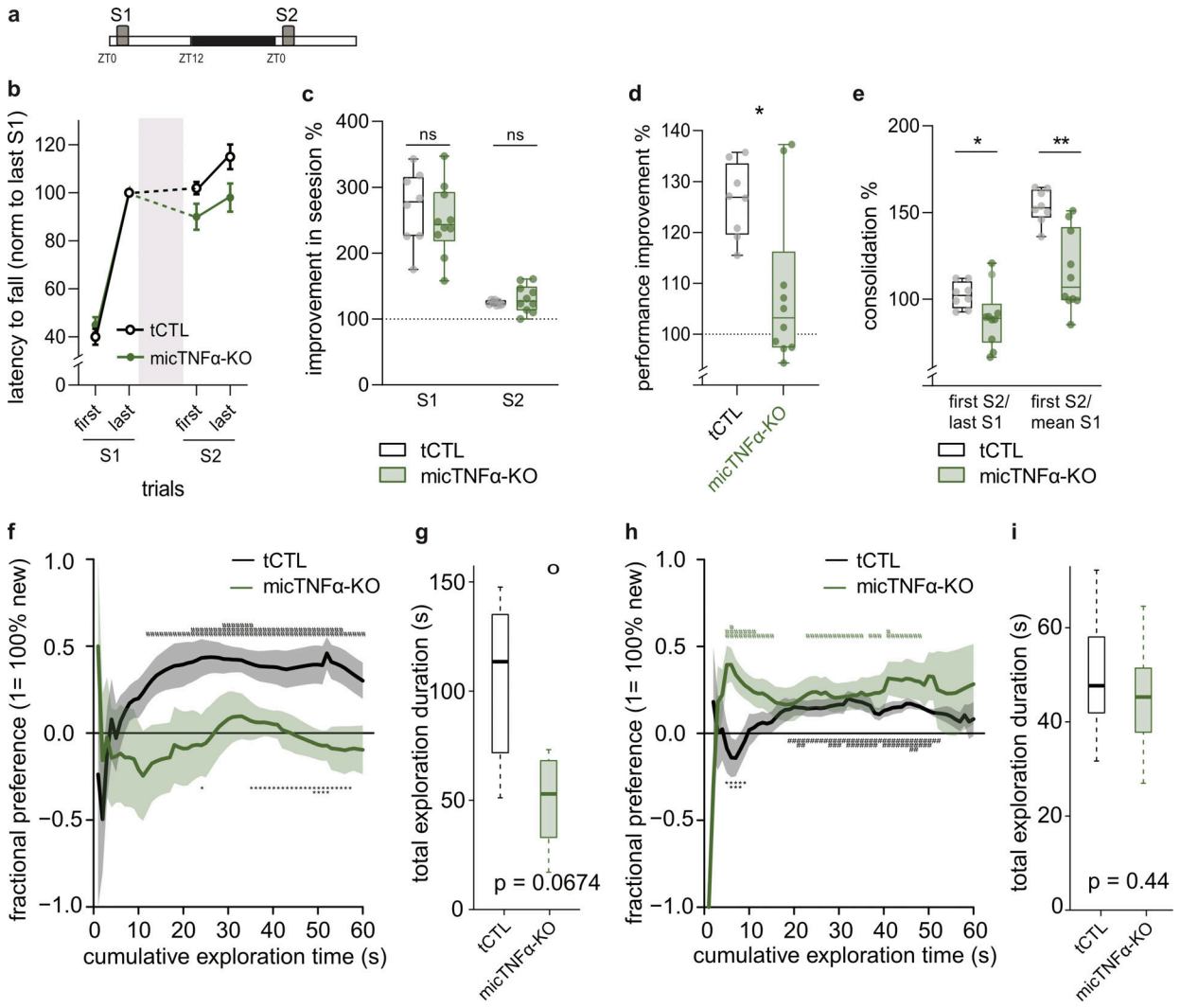

Figure 5. **Microglial TNFα required for memory consolidation in sleep-dependent learning tasks. (a)** Experimental design: Mice learn to run on the complex wheel (session 1, S1) and consolidation of memory is tested the following day (session 2, S2). Between S1 and S2, mice are left undisturbed in their cages. **(b)** Average latency to fall off the complex wheel in the first three and the last three trials of S1 and S2 from tCTL and micTNFα-KO. Gray area represents undisturbed sleep–wake cycle. Dashed line represents S1 to S2 consolidation. 8 tCTL and 10 micTNFα-KO mice. The data represent mean ± SEM. **(c)** Improvement within each session was measured as the ratio between the mean of the best three trials and first three trials. No statistical significance (ns) by unpaired two-tailed Mann–Whitney test. **(d)** Performance improvement across sessions was measured as the ratio between the mean of S2 and S1 trials. *P < 0.05, unpaired two-tailed Mann–Whitney test. **(e)** Consolidation of motor learning across sessions was measured in two ways: the ratio between the mean of the first three trials of S2 and mean of the last three trials of S1 (first S2/last S1) or ratio between mean of first three trials of S2 and mean of S1 trials (first S2/mean S1). *P < 0.05 and **P < 0.01, unpaired two-tailed Mann–Whitney test. **(c–e)** 8 tCTL and 10 micTNFα-KO mice. Results are presented as minimum to maximum box-plots with the individual values of each mouse represented as datapoints. **(f and h)** Novelty preference in the novel floor-texture recognition (FTR) (f) or the Novel Object Recognition (NOR) task (h). Fractional preference is expressed as a function of cumulative time of exploration (see Materials and methods). The data represent the mean ± SEM of the preference for the object placed on the novel floor texture (f) or for the novel object (h) computed for each animal. #P < 0.05, ##P < 0.01, and ###P < 0.001 preference for one object versus no preference and *P < 0.05, **P < 0.01, and ***P < 0.001 CTL versus micTNFα-KO. Unpaired *t* tests. The fractional preference is equal to 1 or −1 when the animal only explored respectively the object placed on the novel or familiar floor texture in the FTR and the novel or familiar object in the NOR, and 0 when the animal spent exactly the same amount of time on the two objects. **(g and i)** Total duration of exploration of the novel floor (FTR; g) and of the novel object (NOR; i). Boxes represent quartiles and whiskers correspond to the range of data; points are singled as outliers if they deviate more than 1.5 × inter-quartile range from the nearest quartile. **(g)** °P = 0.0674 CTL versus micTNFα-KO, Unpaired *t* tests. **(i)** P = 0.44 CTL versus. micTNFα-KO. Unpaired *t* tests; (f–i) *n* = 11 tCTL and 8 (f and g) or 16 (h and i) micTNFα-KO mice.

(Fig. 5 c). This shows that lack of microglial TNFα did not alter complex motor learning, which is known to be sleep-independent (Nagai et al., 2017). We further showed that it does not impair locomotor activity and does not induce anxiety-like behavior as assessed in an open-field task (Fig. S9). We next measured the improvement of performance in the complex motor learning task between S1 and S2 and found that it was higher in tCTL as compared with micTNFα-KO (Fig. 5 d). Finally, we tested the memory consolidation by comparing performance at the beginning of the second session (First S2) with either the last or the mean performance of the first session (Last S1 or Mean S1). Memory consolidation was impaired in mice lacking

microglial TNFα as compared with controls (Fig. 5 e). In this complex motor learning task, the improvement of performance between sessions and memory consolidation are both known to be sleep-dependent processes (Nagai et al., 2017).

To confirm the involvement of microglial TNFα in memory consolidation, tCTL and micTNFα-KO mice performed a floor-texture recognition task, which was known to depend on cortical activity during NREM sleep (Miyamoto et al., 2016b). Mice first explored an arena with a single floor-texture (training session, smooth or rough) and containing two identical objects on each side. After 1 day of ad libitum sleep, mice explored the same arena containing the same two objects which were placed either on a familiar or on a novel floor-texture (testing session, smooth or rough). As expected (Miyamoto et al., 2016b), tCTL mice spent more time exploring the object located on the novel floor-texture during the testing session (Fig. 5 f). In contrast, micTNFα-KO mice explored significantly less the object located on the novel floor-texture (Fig. 5, f and g), confirming the impairment of memory consolidation on these mice.

Finally, tCTL and micTNFα-KO mice were tested in the novel-object recognition task (Fig. 5, h and i). During the sampling session, mice explored two identical objects, and the next day (testing session), one of the original objects was replaced by a novel object. The amount of time taken to explore the novel object during the testing session provides a quantification of memory consolidation. Noteworthy, however, both genotypes exhibited a larger amount of time spent exploring the novel object (Fig. 5 i), indicating normal consolidation for this test.

Discussion

Microglia, the principal immune cells of the brain, are now acknowledged as instrumental in the perception of the external environment (Thion et al., 2018). How microglia actively translate their external sensing into suitable cues to adapt circuitries in the healthy brain is yet unknown. Our results favor a model in which microglia sense neuronal activity through an ATP/P2RX7 signaling pathway and respond to it by releasing TNFα. Microglial TNFα then gates the phosphorylation of neuronal CaMKII that modulates $GABA_AR$ content at layer 1 cortical synapses (Fig. 2). In the light period, microglia act through TNFα to upregulate synaptic $GABA_AR$ content in L1 (Figs. 1 and 3), which likely contributes to the strengthening of inhibitory transmission in the upper cortex (Bridi et al., 2020). In line with the prominent role of inhibition in the generation of slow waves (Funk et al., 2017; Hay et al., 2021; Lemieux et al., 2015; Niethard et al., 2018; Zucca et al., 2017), microglial TNFα shapes slow waves by controlling transition into down states (Fig. 4). We finally demonstrate that microglial TNFα is determinant for memory consolidation in learning tasks previously shown to occur in a sleep-dependent manner (Nagai et al., 2017; Miyamoto et al., 2016b) (Fig. 5).

Our results were obtained from experiments performed both in vivo and in organotypic slices. The latter system closely mimics the in vivo brain by preserving tissue architecture and cellular composition. In these slices, microglia retain their 3D ramified morphology and their functional properties (De Simoni et al., 2008; Delbridge et al., 2020; Weinhard et al., 2018). They further conserve their ability to regulate synapses (Cantaut-Belarif et al., 2017; Pascual et al., 2012). This indicates that functional interactions between neurons and microglia are conserved in organotypic slices. Indeed, in this work, we have identified microglial TNFα, ATP/P2RX7, and CaMKII as molecular actors of synaptic $GABA_ARs$' regulation in organotypic slices, and we have further confirmed their role in vivo in the light versus dark regulation of $GABA_ARs$ plasticity. Notably, our work does not exclude the possible involvement of other cell types such as astrocytes which have already been shown to be TNFα-dependent regulators of synaptic transmission (Santello et al., 2011).

Excitatory synapses are scaled down during sleep through the removal of AMPA receptors to compensate for potentiation due to ongoing learning during wake. Microglia may contribute to downscaling during sleep by eliminating excitatory synapses (Choudhury et al., 2019), a behavior presumably tuned down during wake by noradrenaline (Liu et al., 2019; Stowell et al., 2019). More recently, microglial CX3CR1 signaling was shown to differentially regulate excitatory synaptic transmission along the light/dark cycle (Corsi et al., 2022). We now show that microglia tune a sleep-dependent regulation of inhibitory synapses restricted to cortical layer 1 via mobilization of the P2RX7/TNFα signaling and regulation of synaptic $GABA_AR$ content. Noteworthy, comparable amplitude of changes in the $GABA_AR$ were found in the sleep/wake cycle analysis of the proteome of forebrain synaptosomes (Noya et al., 2019). The layer 1 versus layer 5 specificity may arise from the molecular difference of GABAergic synapses across the somato-dendritic arbor as proposed (Chiu et al., 2018). Alternatively but not exclusively, it may result from a differential expression of TNF-R1 along the cortical layers and/or from layer-specific behavior of microglia (Stogsdill et al., 2022). Altogether, microglia are arising as active players in excitatory and inhibitory synapse remodeling along the sleep/wake cycle, likely to underlie daily oscillations in synaptic strength (Bridi et al., 2020; Tononi and Cirelli, 2019; Vyazovskiy et al., 2008).

Our study suggests that microglia can target specific sets of synapses by acting locally in a sleep-dependent manner; however, the mechanisms supporting this spatiotemporal specificity have remained elusive. Microglia expression of TNFα mRNA peaks in the middle of the light phase (Fonken et al., 2015), when sleep is maximal. Specificity could be achieved by differential microglial production of TNFα; however, our attempt to visualize the distribution of TNFα protein in the cortex at sleep and wake states failed due to the unreliability of anti-TNFα antibodies (not shown). Dynamics of TNFα release by microglia along a light/dark cycle in specific sleep states thus await the advent of suitable tools. Another potential source of specificity may come from sleep-specific patterns of neuronal activity and downstream ATP release that can then engage local microglia. For instance, intense calcium spikes occur during sleep on the apical dendrites of pyramidal neurons inducing plasticity in upper cortical layers (Li et al., 2017). ATP levels in the frontal cortex actually peak in the light period in a sleep-dependent manner (Dworak et al., 2010). Resolving the mechanism

promoting spatiotemporal specificity of microglia functions during sleep would give great insight into microglia-neuronal crosstalk in the physiological brain.

TNFα has long been known as a sleep factor. Administration of exogenous TNFα promotes SWA and NREM sleep (Fang et al., 1997; Yoshida et al., 2004), whereas inhibition of endogenous TNFα reduces NREM sleep (refs in Rockstrom et al., 2018). Similarly, intracerebral or intraperitoneal injection of TNFα (Shoham et al., 1987) suppresses REM sleep, which is increased in a dark period-specific manner in TNFα KO mice (Szentirmai and Kapás, 2019). These results seem to partially contradict our results showing no difference in NREM sleep amount and no dark-specific increased REM sleep in mice with microglia-specific TNFα depletion. However, TNFα injection either directly in the brain (Yoshida et al., 2004) or intraperitoneally (Fang et al., 1997) leads to concentrations that are likely higher than the physiological concentration (Garré et al., 2017), with putative widespread diffusion and off-target and indirect effects. Furthermore, the studies using TNFα or TNFα receptors knockout have not used cell-specific and inducible inactivation, and it is thus difficult to discriminate between a microglial-specific effect to indirect effects due to non-microglial TNFα and/or secondary developmental alterations. Finally, TNFα is also a major mediator of inflammation, which induces sleep dysfunction by yet elusive mechanisms (Irwin, 2019). Our work now provides possible molecular and cellular links between sleep and inflammation.

Cortical inhibition is involved in the control of SWA during NREM sleep (Funk et al., 2017; Zucca et al., 2017; Zielinski et al., 2019) with a prominent role in the onset of down states (Chen et al., 2012; Lemieux et al., 2015). Such control is likely achieved through inhibitory networks in the upper layers of the cortex. Thalamic drive onto L1 inhibitory neurogliaform cells induces transition into down states (Hay et al., 2021). In addition, SOM-IN densely targets L1, and their firing precedes entry into down states (Niethard et al., 2018). Accordingly, SOM-IN chemoactivation increases by about 17% the slope of slow waves and triggers down states (Funk et al., 2017). We found that depletion of microglial TNFα leads to a 17% decrease in the slope of slow waves to down states. Remarkably, the slope of slow waves is under homeostatic control. Indeed, sleep deprivation increases the slope of slow waves (Funk et al., 2017; Hubbard et al., 2020), and in early sleep, when sleep need is high, the slope of the slow waves is steeper by 15% above the average (Vyazovskiy et al., 2007). Therefore, the decrease in slow wave slope in micTNFα-KO mice aligns with our earlier finding that these mice exhibit reduced expression of sleep need (Pinto et al., 2023).

In this study, we show that L1 inhibitory synapses are modulated by microglia in a sleep-dependent manner. Our data favor the possibility that the microglia-targeted GABAergic synapses arise from SOM-IN. However, inhibition on L1 also originates from local axonal arbors of neurogliaform and canopy cells (Schuman et al., 2021), and the identity of the presynaptic neurons remains to be established. In line with their ability to modulate inhibitory synapses in cortical L1, yet without ruling out their possible involvement in other brain regions and/or by other mechanisms, microglia are regulators of slow waves during NREM sleep through TNFα. A causative link between microglia modulation of inhibitory synapses and sleep slow waves awaits future studies. Together with evidence of astrocytic involvement in SWA (Szabó et al., 2017; Vaidyanathan et al., 2021), our work offers insight into how local glial modulation of neuronal networks may tune brain oscillations. Local modifications in SWA within cortical regions involved in learning processes are crucial for learning consolidation and performance improvement (Huber et al., 2004; Hanlon et al., 2009). Our work suggests that microglia could play a role in facilitating the necessary adjustments in SWA during NREM sleep that accompany the intense recruitment of neural networks during learning episodes.

Cortical inhibition controls sleep-dependent memory consolidation (Zielinski et al., 2019), which itself critically depends on slow waves (Fattinger et al., 2017; Marshall et al., 2006). It has even been proposed that one of the major physiological roles of sleep is to allow memory consolidation (Klinzing et al., 2019). We now show that mice lacking microglial TNFα display impaired memory consolidation when tested in a complex rotarod motor learning task or in the floor-texture recognition (FTR) task. In these two tasks, memory consolidation was shown to be sleep-dependent (Nagai et al., 2017; Miyamoto et al., 2016b). However, no deficiency was observed in micTNFα-KO mice when tested on the novel object recognition test. Specific involvement of microglial TNFα in texture but not in object recognition memory suggests that distinct brain circuits may be involved in these distinct recognition tasks. Accordingly, memory consolidation in the FTR task is dependent on the secondary motor cortex S2 inputs to the S1 sensory cortex hind paw area, unlike the object-location recognition task (Miyamoto et al., 2016b). Furthermore, mice lacking neuronal nitric oxide synthase in cortical somatostatin neurons exhibit the same deficit in FTR but not in novel object recognition tasks, providing additional evidence for a region-specific effect (Zielinski et al., 2019).

Finally, this work adds to the yet limited knowledge of microglia functions in the healthy adult brain (Parkhurst et al., 2013; Wang et al., 2020) and establishes microglia as genuine regulators of inhibitory synapses, brain oscillations, and memory in the healthy brain. Noteworthy, microglial regulation likely occurs through the control of CaMKIIα, which is a cardinal regulator of synaptic plasticity (Bayer and Schulman, 2019). It may occur on SOM-IN inputs, which are not only involved in the control of complex behaviors such as sleep but also in decision-making and learning (Adler et al., 2019). Finally, this work demonstrates that microglia tune slow waves and support memory consolidation probably by acting during sleep (Klinzing et al., 2019). We thus anticipate a far wider involvement of microglia in other forms of plasticity and higher brain functions.

Materials and methods

Animals and housing

Mice were housed under standard conditions (12 h light/dark cycle; lights on at 7:00 A.M.). All experiments were performed in conformity with the European Committee Council Directive 86/609/EEC and were approved by the local Charles Darwin Ethical

Committee (Ce5-2014-001; 1339-2015073113467359 and 2018022121466547). CX_3CR1^{GFP} (Jung et al., 2000); $CX_3CR1^{CreERT2}$ (Yona et al., 2013); TNF^{flox} (Grivennikov et al., 2005); P2rx7-KO (Solle et al., 2001); SOM^{iCre} (Taniguchi et al., 2011); and Ai9 (Madisen et al., 2010) mouse lines were housed at the animal facility of Institut de Biologie de l'ENS or the animal facility of Institut Biologie Paris Seine (Paris, France). CX_3CR1^{GFP}, $CX_3CR1^{CreERT2}$, and Ai9 were kindly provided by Sonia Garel (Institut de Biologie de l'Ecole Normale Supérieure, Paris, France), TNF^{flox} by Etienne Audinat (Institute of Functional Genomics, Montpellier, France), and P2X7R-KOs by François Rassendren (Institute of Functional Genomics, Montpellier, France). C57BL/6J pregnant females and wild-type males were obtained from Janvier Labs.

Brain organotypic slices

Brain organotypic slices were prepared as previously described (Hill et al., 2014). Brains were removed from P3–P7 C57BL/6J mice (wild-type, $CX_3CR1^{+/+}$:$TNF^{f/f}$ or $CX_3CR1^{CreERT2/+}$:$TNF^{f/f}$), and the hemispheres were separated in a dissection medium (33 mM glucose in PBS). Coronal slices (350 µm) were cut using a McIllwain tissue chopper (Mickle Laboratory) and placed on Millicell cell culture inserts (Millipore, PICM03050) (two to three slices per insert). Slices were maintained at 37°C in 5% CO_2/air for 14–21 days in MEM (21090-022; GIBCO) supplemented with 20% heat-inactivated horse serum (16050-122; GIBCO), 2 mM glutamine, 10 mM glucose, 20 mM HEPES, 10 U/ml penicillin, and 10 µg/ml streptomycin. The culture medium was changed three times per week.

Adult primary microglia cultures

Isolation of primary microglia from adult mouse brain was performed as previously described (Lee and Tansey, 2013). In brief, adult mice were anesthetized by inhalation of isoflurane and transcardially perfused with 10 ml PBS. Brains were individually dissociated in a solution containing 30–40 U papain (LK003176; Worthington), 7.2 U dispase II (D4693; Sigma-Aldrich), and 10 mg/ml DNAse (DN25; Sigma-Aldrich), followed by mechanical dissociation. Microglia were isolated by collecting the 70–37% interphase of a Percoll gradient (P4937; Sigma-Aldrich) and plated on poly-ornithine-coated plates in DMEM/F12 (31331-028; GIBCO) supplemented with 10% heat-inactivated fetal bovine serum (10500-064; GIBCO), 10 U/ml penicillin, and 10 µg/ml streptomycin.

Spleen cultures

Adult mice were anesthetized by inhalation of isoflurane and transcardially perfused with 10 ml PBS, followed by dissection of the spleen and its dissociation in 150 mM NH_4Cl, 10 mM $NaHCO_3$, and 0.1 mM EDTA solution. Spleen cells were kept in culture in DMEM (61965-026; GIBCO) supplemented with 10% heat-inactivated fetal bovine serum (10500-064; GIBCO), 1 mM sodium pyruvate, 10 U/ml penicillin, and 10 µg/ml streptomycin.

Treatments

The drugs and neutralizing or activating antibodies used in this study are listed in Table S3. Treatments to brain organotypic slices in culture were performed as follows. For long-term treatment with PLX3397 (7–9 days), Mac1-saporin (7 days) and 4-hydroxytamoxifen (12–15 days), the drug and vehicle, respectively, were added to the culture medium at each medium change. All other treatments were performed between days in vitro (DIV) 16–20 in prewarmed artificial cerebrospinal fluid (aCSF; 125 mM NaCl, 2.5 mM KCl, 2 mM $CaCl_2$, 1 mM $MgCl_2$, 5 mM HEPES, 33 mM glucose, pH 7.3). To guarantee rapid penetration of the drugs into the tissue, slices were immersed in aCSF during treatments (final volume of 2 ml, 1 ml under, and 1 ml inside the insert). Induction of iLTP was accomplished by a 2-min treatment with NMDA and CNQX followed by 20 min recovery in NMDA/CNQX-free aCSF. BzATP treatment followed the same temporal pattern as iLTP. Whenever indicated, drugs were added before (preincubation of 15 min [for A740003, apyrase, fluoroacetate, KN62, minocycline, and neutralizing and activating antibodies, PPADS and PSB0739] or 40 min [TAPI-1]) and during iLTP or BzATP treatment. For drugs diluted in DMSO, a 1,000× concentrated stock was used, and an equal volume of DMSO was added to the controls. To remove contaminating K^+ from apyrase (Madry et al., 2018), dialysis was done in 0.025 µm pore nitrocellulose membranes (VSWP01300; Millipore).

For immunohistochemistry purposes, brain organotypic slices were fixed in 2% PFA (15710-S; Electron Microscopy Sciences) in PBS for 1 h at 4°C and washed three times with PBS. For immunostainings of synaptic markers, organotypic slices were cryopreserved on 20% sucrose for at least 24 h at 4°C and cut on a cryostat to 14 µm-thick sections. Following the normal flattening of organotypic slices in culture, slices were ∼150–200 µm thick at the time of fixation, allowing us to cut between 9 and 12 cryostat 14 µm-thick sections per each organotypic slice.

Analysis of sleep–wake synaptic plasticity

Sleep–wake experiments were carried out in 12- to 15-wk-old C57BL/6J males kept on a 12 h:12 h light/dark cycle. Wild-type mice were fed with normal or PLX3397-containing food (290 mg PLX3397 in 1 kg standard chow, formulated by SSNIFF, S9555-P710) for 2 wk. Microglia-TNFα depleted mice (micTNFα-KO, $CX3CR1^{CreERT2/+}$:$TNF^{f/f}$) and transgenic controls (tCTL, $CX3CR1^{GFP/+}$:$TNF^{f/f}$) were fed with tamoxifen-containing food (1,000 mg tamoxifen citrate in 1 kg of chow, formulated by SSNIFF, A115-T71000) for 6 days. Sleep–wake experiments were performed 2 wk after tamoxifen feeding to allow the repopulation of short-lived peripheral $CX3CR1^+$ cells, thus restricting recombination to microglia (Yona et al., 2013; Goldmann et al., 2013). ZT6 and ZT18 mice were kept undisturbed in their cages and taken in the middle of the light period and the middle of the dark period, respectively. Enforced wake was accomplished by gentle introduction of novel objects inside the cage and gentle tapping of the cage for 6 h starting at the onset of the light period (Colavito et al., 2013). At the indicated times, mice were collected and rapidly anesthetized by inhalation of isoflurane, followed by transcardial perfusion with 2% PFA. Brains were dissected, postfixed at RT for 6 h in 2% PFA (15710-S; Electron Microscopy Sciences), and cryopreserved on 20% sucrose for 5 days at 4°C. Brains were rapidly frozen and sagittal sections of the left

hemisphere were cut on a cryostat at 9 µm thickness for further immunostaining. To guarantee a good sampling, six sagittal sections (distancing at least 100 µm in the brain tissue) were collected per brain onto the same slide and used for imaging.

Immunohistochemistry (IHC)

Cryostat sections were submitted to blocking and permeabilization in 0.25% gelatin–0.1% triton and incubated with primary antibodies at 4°C overnight with shaking. Slices were washed in PBS-0.1% triton (4 × 15 min) and then incubated with secondary antibodies at RT for 3 h with shaking. All secondary antibodies conjugated to fluorophores (Alexa Fluor 488, Cy3 or Alexa Fluor 647) used were from Jackson ImmunoResearch and diluted 1:500. Slices were washed in PBS-0.1% Triton (4 × 15 min) and mounted on Vectashield mounting medium (H-1000; Vector Laboratories) containing DAPI (D3571; Invitrogen).

Whenever indicated (see Table S4), decloaking chamber-based heat-induced epitope retrieval (HIER) was performed before immunostaining. Sections were processed in a decloaking chamber (model DC2008INTL; Biocare Medical) at 110°C for 20 min in an antigen decloaker solution (CB910M; Biocare Medical), incubated at RT for 15 min with 15% methanol 0.3% H_2O_2 in PBS, and incubated at RT for 40 min in 1% sodium borohybride in PBS (solution prepared fresh between 45 min and 2 h before use) with shaking. Slices were then immunostained as previously described.

The antibodies and immunohistochemical methods used in this study are listed in Table S4.

Confocal imaging and quantitative analysis

For imaging of synaptic clusters in organotypic slices, a Leica SP8 inverted confocal microscope equipped with a 63× glycerol objective (1.4 NA), a hybrid detector, and the Leica Application Suite X (LAS X) software was used. Single confocal plane images were taken to cortical L1 or putative cortical L5 with a 3× zoom factor applied (512 × 512 pixels, pixel size of 120 nm). Images were taken of three to five cryostat sections obtained from two to three organotypic slices for each condition of an independent experiment. For imaging of synaptic clusters in adult brain tissue, a Leica SP5 upright confocal microscope equipped with a 63× oil objective (1.4 NA), a hybrid detector, and the Leica Application Suite X (LAS X) software was used. Images taken were 1 µm z-stacks of three confocal planes (*z* resolution 0.5 µm) with a 4× (at L1) or 5× (at L5) zoom factor applied. Images were taken to the frontal cortex (between 0.5 and 2 mm lateral to midline and >2 mm anterior to bregma) from six cryostat sections for each brain. All imaging was performed at room temperature in a bidirectional manner at 200 Hz speed.

Double or triple colocalization analysis of synaptic clusters was performed automatically on ICY software (de Chaumont et al., 2012) by a custom-built protocol. Analysis was done on either images of a single confocal plane (organotypic slices) or sum projections of z-stacks (adult brain). First, clusters in each channel were detected by the Spot Detector block (Olivo-Marin, 2002), which extracts spots based on an undecimated wavelet transform detector (size of spots set to scales two or three; threshold values kept constant for each experiment). Identification of colocalization events between detected clusters was accomplished by the object-based colocalization Studio block using the Statistical Object Distance Analysis (SODA) software. In brief, a fixed distance (set to between 500 and 600 nm) from the center of mass of each detected cluster is used to detect colocalization events with clusters from another channel (Lagache et al., 2018). For each channel, detected clusters were then pooled into colocalized and non-colocalized, and their total number and individual intensity values were extracted. In triple-colocalization, a cluster is considered as colocalized when colocalization was detected with the two other channels individually. For instance, a $GABA_AR$ cluster is considered synaptic when colocalized with gephyrin clusters or both gephyrin and VGAT clusters for double or triple colocalization, respectively. A $GABA_AR$ cluster is considered extrasynaptic when it shows no colocalization with any of the synaptic markers used. To reduce variability due to uneven background intensity, local background subtraction was applied to each individual cluster.

ELISA for TNFα

Following 4-hydroxytamoxifen treatment, $CX_3CR1^{+/+}$:$TNF^{f/f}$ or $CX_3CR1^{CreERT2/+}$:$TNF^{f/f}$ organotypic slices were treated with LPS for 3 h in aCSF, lysed in cell extraction buffer (10 mM Tris, 100 mM NaCl, 1 mM EDTA, 1% Triton X-100, 10% glycerol, 0.1% SDS supplemented fresh with 1 mM NaF, 2 Mm Na_3VO_4 and protease inhibitor cocktail [05056489001; Roche]) by mechanical dissociation, centrifuged for 10 min at 16,000 *g* at 4°C, and the supernatant was collected. Adult primary microglia were plated in 96-well plates (40,000 cells per well) and stimulated with LPS or BzATP for 6 h. Spleen cells were plated in 24-well plates (3,000,000 cells per well), allowed to deposit for 2 h, and stimulated with LPS for 24 h. For both microglia and spleen cells, the medium was collected and centrifuged for 5 min at 10,000 *g* at 4°C, and the supernatant was collected. Levels of TNFα in the samples were determined by the mouse TNFα uncoated ELISA kit (88-7324; Invitrogen).

Western blot

For Western blot analysis of CaMKII phosphorylation, organotypic slices were homogenized in cell extraction buffer by mechanical dissociation, centrifuged for 10 min at 16,000 *g* at 4°C, and the supernatant was collected. Total protein concentration was determined by the Pierce BCA protein assay kit (23225; Thermo Fisher Scientific). Samples (40 µg of protein) were denatured at 95°C for 5 min in a denaturating buffer (125 mM Tris-HCl, 10% glycerol, 2% SDS, bromophenol blue, and 5% β-mercaptoethanol added fresh), resolved by SDS-PAGE in 8% polyacrylamide gel, and transferred to PVDF membranes. Membranes were blocked in 5% dry milk and incubated with primary antibody against phosphoT286-CamKII (1:1,000, ab171095; Abcam) at 4°C overnight. Membranes were incubated with HRP-conjugated secondary antibody at RT for 1 h. Proteins were visualized by chemiluminescence using SuperSignal West Femto Maximum Sensitivity substrate (34095; Thermo Fisher Scientific) and scanned on an ImageQuant LAS 4000 imaging system (GE Healthcare). Membranes were stripped with 0.2 M NaOH for 40 min, reprobed for total CamKII (1:1,000, ab22609;

Abcam), and resolved with Lumi-Light Western blotting substrate (12015196001; Roche). Quantification was performed on ImageJ.

Electrode implantations for sleep monitoring

Mice were anesthetized with ketamine/xylazine before being fixed in a stereotaxic apparatus. All coordinates were adapted from the mouse brain atlas (Franklin and Paxinos, 2008).

Mice were implanted with the classical set of electrodes (made of enameled nichrome wire, 150 µm in diameter) for polygraphic sleep monitoring (Henderson et al., 2017). Briefly, two electrodes were positioned epidurally in holes perforated into the skull: one electrode was inserted over the frontal cortex (2 mm lateral to midline and 2 mm anterior to bregma; left hemisphere), and one electrode was inserted over the cerebellum. Two electrodes were inserted into the neck muscles. This configuration provided a frontal electroencephalogram (EEG) derivation and an electromyogram (EMG) derivation. All electrodes were soldered to a miniconnector (Antelec). Dental acrylic cement was used to anchor the electrodes to the skull. Mice were allowed to recover for 14 days before starting the administration of tamoxifen-containing food for 6 days or PLX3397-containing food for 2 wk. Mice were placed in individual recording chambers and connected to the recording system with a light-weight cable and a swivel allowing free movements. Recordings started 2 wk after tamoxifen administration.

Sleep recording and analysis

A 24-h baseline (BL) recording starting at dark onset was done to analyze sleep–wake stages in (1) $CX3CR1^{CreER2}$:$TNF^{f/f}$ (micTNFα-KO) and $CX3CR1^{GFP/+}$:$TNF^{f/f}$ (control) mice and (2) wild-type mice fed with normal or PLX3397-containing food for 2 wk. EEG and EMG signals were amplified (2,000×), filtered, digitized at 2,000 Hz, and subsequently downsampled to 200 Hz by an Embla Module acquisition hardware and the Somnologica acquisition software (Medcare). Polysomnographic recordings were visually scored offline for consecutive 10-s epochs as wake, non REM sleep (NREMS), or REM sleep (REMS) as previously described (Henderson et al., 2017). Briefly, wake was defined by low-amplitude/high-frequency EEG activity and elevated EMG tone. NREMS was defined by high-amplitude/low-frequency (<4 Hz) EEG activity and low EMG tone. REMS was characterized by an EEG activity with theta oscillations and a complete absence of EMG tone with occasional twitches. Bouts were defined as consecutive 10-s epochs of similar vigilance state and could be as short as one epoch. Vigilance states amounts for each animal were expressed as minutes per 2- or 12-h intervals or 24-h. Sleep architecture was assessed by calculating the bout mean duration and number for each vigilance state.

Spectral analysis

A spectrogram was first computed using the modulus of the Fast Fourier Transform of 512 EEG samples at 200 Hz (bouts of 2.56 s) multiplied by a Hanning window; the spectral density for each vigilance state was taken as the median of the spectrogram for all EEG bouts belonging to the vigilance state.

Slow-waves analysis

Slow waves were analyzed along the 24 h time period. The EEG was first band-pass filtered using a 0-phase Butterworth filter (0.1–4 Hz, order 2). The slow waves (SW) were defined as NREMS events accompanied by a large and slow positive deflection of the EEG measured against a reference placed over the cerebellum. We first identified as slow positive peaks of the band-pass filtered signal with the 0-crossings surrounding the peaks of the filtered signal separated by more than 0.4 s and <2 s. Amongst these peaks, the SW were selected as the positive oscillations in NREMS larger than a threshold corresponding to $m+3\,s$, where m is the median of the positive peaks of the filtered EEG during wake and s is the difference between the quantiles 0.5 and 0.84 of these peaks; m and s coincide with the mean and the standard deviation if the peak amplitude values would be normally distributed, but this threshold is less sensitive to occasional recording artifacts in the EEG during wake. The relevance of this definition to track events associated with cortical down-states is confirmed in Fig. S8.

The average SW traces were obtained by averaging the EEG centered on the peaks of filtered EEG; the duration of the positive peaks was derived from the time delay between the downward and upward 0-crossing of the filtered EEG around the peaks.

Linear trans-cortical electrodes

To confirm the correspondence between the SW as detected by the procedure above with cortical down-states, we implanted 64 channel linear electrodes (ASSY-156-H3; Cambridge Neurotech, 64 channels interspaced by 20 µm) in the motor cortex of two C57Bl/6J mice. The operations were carried out under isoflurane anesthesia with the aid of an operating microscope. The body temperature was maintained constant during the surgery (36°C) using a heating pad controlled by a rectal thermometer. General analgesia was assured by subcutaneous injection of buprenorphine (3 mg/kg), whereas local analgesia of the skin and skull was provided via subcutaneous injection of lidocaine (0.5 ml of 2 mg/ml solution). Lidocaine spray (10%) was used for the ears, before setting the mouse in the stereotaxic frame (Kopf Instruments). After the povidone–iodine (100 mg/ml) and ethanol (70%) disinfection of the surgical area, a sagittal incision of the scalp was performed. Following exposure of the skull, burr holes were drilled above the studied structures. All coordinates (medio-lateral and antero-posterior) were taken relative to bregma, while the depth was measured starting from the dura mater. The electrode was lowered perpendicular to the cortical surface at the coordinates AP: 1.1 mm, ML: −0.9 mm, z: −1.28 mm, and the surface was covered with Dura-Gel (Cambridge NeuroTech), the rest of the implant is cemented with dental cement onto the skull after having applied a thin layer of superbond on it. A miniature stainless steel screw was implanted over the cerebellum, serving as an electrical reference and ground. The skin ridges were sutured around the connector, and mice were allowed to recover in their home cage for at least 7 days. The implanted mice were housed individually in standard cages. Mice were recorded with the Intan RHD USB interface board as a recording setup (at sampling frequency 30 kHz) in a round

openfield (40 × 40 cm) where the nest of the home cage was transferred during 2 h at noon.

Linear electrodes processing

The signal from the linear electrodes was decomposed offline in LFP using forward and reverse pass filtering with a low-pass filter (0.1–150 Hz Butterworth filter of order 2) and in multi-unit activity. The SWs were identified using the same procedure as for EEG applied to the LFP signal from the surface channel of the linear electrodes. The multiunit activity was extracted off-line by first performing a forward and reverse pass of filtering with a high-pass filter (500 Hz–8 kHz, Butterworth filter of order 2), and second, extracting the multiunit spikes selected as the transient negative events deviating more than six times the standard deviation of the high-pass filtered signal. The peak of the SW LFP traces was detected from the delta-filtered signal.

Open-field test

Mice were placed at the center of an open-field arena (50 × 50 cm) and were allowed to explore it for 15 min. The open-field was divided into a central area (17 × 17 cm) and a peripheral area. Mice were video-tracked with Ethovision software 14.0 by Noldus and the distance moved, velocity, and time spent in the central area were analyzed for 15 min.

Complex wheel task

Sleep-dependent consolidation of motor learning was assessed by the complex wheel task as previously described (Nagai et al., 2017). A complex wheel with missing rungs (bar pattern as in Nagai et al., 2017) was mounted on a rotarod. tCTL and micTNFα-KO mice with no habituation or pretraining on the rotarod were used. Two learning sessions (S1 and S2) were done 24 h apart at ZT1, the beginning of the light period. S1 and S2 consisted of 20 and 19 trials, respectively, on the complex wheel with an acceleration increasing from 0 to 40 rpm in 10 min. Mice were allowed a 5 min rest in their cages between each 10 trials. For each trial, the latency to fall corresponds to the time the mouse kept running on the complex wheel without falling. For each mouse, latency to fall off the complex wheel in each S1 and S2 trials was normalized to the average of the last three trials in S1. The normalized values were used to plot the graphs in Fig. 5. Considering that memory consolidation of mice with poorer performances on the complex wheel is less impacted by sleep deprivation than skilled learners (Nagai et al., 2017), only the best learners within each group were taken into consideration for the analysis. Within each group (tCTL and micTNFα-KO), the best learners correspond to the mice that on S1 performed better than the median of the average performance in all trials. The experimenter was blind to the genotypes.

Memory recognition tasks

Sleep-dependent consolidation of recognition memory (Miyamoto et al., 2016b; Rolls et al., 2011) was assessed by the novel floor-texture recognition (FTR) and novel object recognition (NOR) tasks. FTR and NOR tasks were performed in a square open field (42 cm) and started at ZT3. Both tasks were based on innate novelty preference in mice. Habituation consisted of (1) a 30-min exploration period of the open field with cagemates (Day1), (2) a 15-min period during which each mouse was placed individually in the empty open field (Day2), and (3) a 15-min period during which the mice were placed in the open-field with two identical objects (Day3). The tests were executed in the following order: the FTR task was performed on days 4 and 5 and the NOR test on days 6 and 7. On the FTR training session (Day4), mice were allowed to explore two new identical objects in the arena containing a single floor texture (smooth or rough plexiglas) for a 5-min period. This was repeated 2 times (3 × 5-min exploration period in total). On the testing session (Day5), the mice were tested for the FTR paradigm (5 min) during which the arena contains the same two objects but two floor-textures (smooth and rough) on opposing halves of the floor. On the NOR training session (Day 6), mice were allowed to explore two new identical objects for a 5-min period. This was repeated two times (3 × 5-min exploration period in total). On the testing session (Day 7), the mice were tested for the NOR paradigm (5 min) during which one of the original objects was replaced with a new object. At the end of each session, mice were replaced and remained in their home cage for 24 h. Mice that did not accumulate 10 s of total inspection time per object over two training sessions in the FRT or the NOR tests were excluded.

Since novelty preference may take some time to become visible (e.g., if the animal takes some time to begin the exploration of one of the two options available) but shall decay along extended exploration (when the novel situation becomes familiar), we chose to examine the object preference as a function of the cumulative time of exploration in the session. For this purpose, we first assessed the amount of time spent exploring each object per 10-s epochs using the Ethovision software 14.0. Then, we computed the object preference as a function of the cumulative time of exploration. For each animal, $v_{nov}(t_i)$ and $v_{fam}(t_i)$ correspond to the amount of time the mouse, at the time in the session t_i, spent exploring respectively the object placed on the novel or familiar floor texture in the FTR and the novel or familiar object in the NOR. For each epoch, we compute the cumulative time of exploration T_j, $T_j = \sum_{t_i < t_0^j} v_{nov}(t_i) + v_{fam}(t_i)$ and the object preference $p(T_j)$ as $p(T_j) = \left(\sum_{t_i < t_0^j} v_{nov}(t_i) - v_{fam}(t_i) \right) \Big/ T_j$ which value shall be 1 or −1 if the animal only explored respectively the object placed on the novel or familiar floor texture in the FTR and the novel or familiar object in the NOR, and 0 if the animal spent exactly the same amount of time on the two objects. The object preference values are linearly interpolated by a step of 1 s (of cumulated exploration time) to compute the average/SEM across animals.

Statistical analysis

Statistical significance was defined as follows: ns, not significant ($P > 0.05$); ***$P < 0.001$; **$P < 0.01$; and *$P < 0.05$.

$GABA_AR$ plasticity

Results are presented as minimum to maximum box plots. Graphs and statistical analysis were performed in Prism 8.0

(GraphPad software). Statistical significance was assessed by nonparametric tests or by nested statistical analysis. For the latter, data distribution was assumed to be normal, but this was not formally tested. For comparisons of changes between two groups, nested two-tailed *t* test or Kolmogorov–Smirnoff test (for cumulative distributions) was performed. For comparisons between multiple groups, nested one-way ANOVA followed by Sidak's multiple comparison test or Kruskal–Wallis test followed by Dunn's multiple comparisons test was used.

Sleep recordings

Sleep data were analyzed using Prism 9.3 (GraphPad Software). Normality and homoscedasticity assumptions were verified prior to the use of any parametric tests (D'Agostino-Pearson normality test or Shapiro–Wilk test and equality of variances F-test). Data violating normality were log transformed. Statistics was performed with repeated measures two-way ANOVAs to test the significance between genotypes (tCTL and micTNFα-KO) or treatment (normal or PLX3397-containing food) and time (repeated measures over 2-h segments) for wake, REMS, and NREMS. When appropriate, ANOVAs were followed by the Sidak's multiple comparisons test between genotypes. Two-tailed unpaired *t* test or Mann–Whitney test were also employed to assess the significance of the effects of the genotype or treatment on the different variables (amounts, bout mean durations, numbers of bouts) per 12- or 24-h.

Online supplemental material

Fig. S1 shows the modulation of synaptic and extrasynaptic AMPARs across the light/dark cycle in the frontal cortex. Fig. S2 shows the effects of microglial depletion by PLX3397 on microglial density as well as on $GABA_A$Rs and the amount of vigilance states. Fig. S3 shows that the somatostatin-positive inputs are similarly distributed in the adult brain and organotypic slices. Fig. S4 shows that microglia are required for the iLTP-induced increase in synaptic $GABA_A$Rs but no requirement of CX3CL1 signaling. Fig. S5 confirms the involvement of TNFα in the control of $GABA_A$Rs plasticity. Fig. S6 shows that BzATP increases synaptic $GABA_A$R in a microglia- and CaMKII-dependent manner. Fig. S7 supports the notion that microglia control synaptic $GABA_A$R and CaMKII phosphorylation fluctuations throughout the light/dark cycle. Fig. S8 shows that slow waves coincide with cortical down-states and that the peak upward slope of the slow waves corresponds to the onset of down-states. Fig. S9 shows no alteration in locomotor activity and anxiety-like behaviors in micTNFα-KO mice. Table S1 shows sleep and wake characteristics in control and PLX3397 treated mice. Table S2 shows sleep and wake characteristics in control and micTNFα-KO mice. Table S3 is the list of the drugs and neutralizing or activating antibodies that were used in this study. Table S4 shows the list of antibodies and immunohistochemical methods used in this study.

Data availability

The data underlying all images and graphs are available from the corresponding authors upon request.

Acknowledgments

We are grateful to Amandine Delecourt, Eleonore Touzalin, and Deborah Souchet for their excellent technical assistance. We thank Sonia Garel (IBENS, Paris), Etienne Audinat (Institut de génomique fonctionnelle, Montpellier), and Lauriane Ulmann and François Rassendren (Institut de génomique fonctionnelle, Montpellier) for providing $CX_3CR1^{CreERT2}$ and Ai9; TNF^{flox} and P2rx7 -KOs respectively. We are grateful to the IBPS Animal facility for breeding and care, the IBPS-NPS Phenotypic core facility, and particularly Jean Vincent.

This work was funded by: Agence nationale pour la recherche: SYNTRACK -R17096DJ (A. Triller); Agence nationale pour la recherche:EXPECT 17-CE37-0022-2 (C. Léna, D. Popa); European Research Council: PLASTINHIB Project No: 322821 and MICROCOPS (A. Triller); Human Brain Project: HBP SGA2-OPE-2018-0017 (A. Triller); and EMBO fellowship: ALTF 362-2017 (M.J. Pinto). We gratefully acknowledge Astou Tangara, Benjamin Mathieu, and the IBENS imaging facility (IMACHEM-IBiSA), member of the French National Research Infrastructure France-BioImaging (ANR-10-INBS-04), which received support from the "Fédération pour la Recherche sur le Cerveau—Rotary International France" (2011) and from the program « Investissements d'Avenir » ANR-10-LABX-54 MEMOLIFE.

Author contributions: Conceptualization: A. Bessis, A. Triller, C. Léna, D. Popa, M.J. Pinto, V. Fabre. Formal Analysis: C. Léna, M.J. Pinto, and V. Fabre. Funding acquisition: A. Bessis, A. Triller, C. Léna, D. Popa, and V. Fabre. Investigation: J.M.J. Fabre, F. Henderson, L. Bizien, M.J. Pinto, N. Đukanović, V. Fabre, A. Bessis, M. Pujol, R.W. Sala, and T. Tarpin. Software: C. Léna, V. Lepetz, and M.J. Pinto. Writing—original draft: A. Bessis, M.J. Pinto. Writing—review & editing: A. Bessis, A. Triller, C. Léna, D. Popa, M.J. Pinto, V. Fabre, and R.W. Sala.

Disclosures: The authors declare no competing financial interests.

Submitted: 19 January 2024
Revised: 18 March 2024
Accepted: 28 March 2024

References

Adamantidis, A.R., C. Gutierrez Herrera, and T.C. Gent. 2019. Oscillating circuitries in the sleeping brain. *Nat. Rev. Neurosci.* 20:746–762. https://doi.org/10.1038/s41583-019-0223-4

Adler, A., R. Zhao, M.E. Shin, R. Yasuda, and W.-B. Gan. 2019. Somatostatin-expressing interneurons enable and maintain learning-dependent sequential activation of pyramidal neurons. *Neuron.* 102:202–216.e7. https://doi.org/10.1016/j.neuron.2019.01.036

Badimon, A., H.J. Strasburger, P. Ayata, X. Chen, A. Nair, A. Ikegami, P. Hwang, A.T. Chan, S.M. Graves, J.O. Uweru, et al. 2020. Negative feedback control of neuronal activity by microglia. *Nature.* 586:417–423. https://doi.org/10.1038/s41586-020-2777-8

Bayer, K.U., and H. Schulman. 2019. CaM kinase: Still inspiring at 40. *Neuron.* 103:380–394. https://doi.org/10.1016/j.neuron.2019.05.033

Beattie, E.C., D. Stellwagen, W. Morishita, J.C. Bresnahan, B.K. Ha, M. Von Zastrow, M.S. Beattie, and R.C. Malenka. 2002. Control of synaptic strength by glial TNFalpha. *Science.* 295:2282–2285. https://doi.org/10.1126/science.1067859

Black, R.A., C.T. Rauch, C.J. Kozlosky, J.J. Peschon, J.L. Slack, M.F. Wolfson, B.J. Castner, K.L. Stocking, P. Reddy, S. Srinivasan, et al. 1997. A

metalloproteinase disintegrin that releases tumour-necrosis factor-alpha from cells. *Nature*. 385:729–733. https://doi.org/10.1038/385729a0

Bridi, M.C.D., F.-J. Zong, X. Min, N. Luo, T. Tran, J. Qiu, D. Severin, X.-T. Zhang, G. Wang, Z.-J. Zhu, et al. 2020. Daily oscillation of the excitation-inhibition balance in visual cortical circuits. *Neuron*. 105: 621–629.e4. https://doi.org/10.1016/j.neuron.2019.11.011

Cantaut-Belarif, Y., M. Antri, R. Pizzarelli, S. Colasse, I. Vaccari, S. Soares, M. Renner, R. Dallel, A. Triller, and A. Bessis. 2017. Microglia control the glycinergic but not the GABAergic synapses via prostaglandin E2 in the spinal cord. *J. Cell Biol.* 216:2979–2989. https://doi.org/10.1083/jcb.201607048

Chen, J.-Y., S. Chauvette, S. Skorheim, I. Timofeev, and M. Bazhenov. 2012. Interneuron-mediated inhibition synchronizes neuronal activity during slow oscillation. *J. Physiol.* 590:3987–4010. https://doi.org/10.1113/jphysiol.2012.227462

Chiu, C.Q., J.S. Martenson, M. Yamazaki, R. Natsume, K. Sakimura, S. Tomita, S.J. Tavalin, and M.J. Higley. 2018. Input-specific NMDAR-dependent potentiation of dendritic GABAergic inhibition. *Neuron*. 97:368–377.e3. https://doi.org/10.1016/j.neuron.2017.12.032

Choudhury, M.E., K. Miyanishi, H. Takeda, A. Islam, N. Matsuoka, M. Kubo, S. Matsumoto, T. Kunieda, M. Nomoto, H. Yano, and J. Tanaka. 2019. Phagocytic elimination of synapses by microglia during sleep. *Glia*. 68: 44–59. https://doi.org/10.1002/glia.23698

Colavito, V., P.F. Fabene, G. Grassi-Zucconi, F. Pifferi, Y. Lamberty, M. Bentivoglio, and G. Bertini. 2013. Experimental sleep deprivation as a tool to test memory deficits in rodents. *Front. Syst. Neurosci.* 7:106. https://doi.org/10.3389/fnsys.2013.00106

Corsi, G., K. Picard, M.A. di Castro, S. Garofalo, F. Tucci, G. Chece, C. Del Percio, M.T. Golia, M. Raspa, F. Scavizzi, et al. 2022. Microglia modulate hippocampal synaptic transmission and sleep duration along the light/dark cycle. *Glia*. 70:89–105. https://doi.org/10.1002/glia.24090

de Chaumont, F., S. Dallongeville, N. Chenouard, N. Hervé, S. Pop, T. Provoost, V. Meas-Yedid, P. Pankajakshan, T. Lecomte, Y. Le Montagner, et al. 2012. Icy: An open bioimage informatics platform for extended reproducible research. *Nat. Methods*. 9:690–696. https://doi.org/10.1038/nmeth.2075

De Simoni, A., N.J. Allen, and D. Attwell. 2008. Charge compensation for NADPH oxidase activity in microglia in rat brain slices does not involve a proton current. *Eur. J. Neurosci.* 28:1146–1156. https://doi.org/10.1111/j.1460-9568.2008.06417.x

Defer, N., A. Azroyan, F. Pecker, and C. Pavoine. 2007. TNFR1 and TNFR2 signaling interplay in cardiac myocytes. *J. Biol. Chem.* 282:35564–35573. https://doi.org/10.1074/jbc.M704003200

Del Cid-Pellitero, E., A. Plavski, L. Mainville, and B.E. Jones. 2017. Homeostatic changes in GABA and glutamate receptors on excitatory cortical neurons during sleep deprivation and recovery. *Front. Syst. Neurosci.* 11: 17. https://doi.org/10.3389/fnsys.2017.00017

Delbridge, A.R.D., D. Huh, M. Brickelmaier, J.C. Burns, C. Roberts, R. Challa, N. Raymond, P. Cullen, T.M. Carlile, K.A. Ennis, et al. 2020. Organotypic brain slice culture microglia exhibit molecular similarity to acutely-isolated adult microglia and provide a platform to study neuroinflammation. *Front. Cell. Neurosci.* 14:592005. https://doi.org/10.3389/fncel.2020.592005

Diering, G.H., R.S. Nirujogi, R.H. Roth, P.F. Worley, A. Pandey, and R.L. Huganir. 2017. Homer1a drives homeostatic scaling-down of excitatory synapses during sleep. *Science*. 355:511–515. https://doi.org/10.1126/science.aai8355

Dissing-Olesen, L., J.M. LeDue, R.L. Rungta, J.K. Hefendehl, H.B. Choi, and B.A. MacVicar. 2014. Activation of neuronal NMDA receptors triggers transient ATP-mediated microglial process outgrowth. *J. Neurosci.* 34: 10511–10527. https://doi.org/10.1523/JNEUROSCI.0405-14.2014

Dixon, C.L., N.L. Harrison, J.W. Lynch, and A. Keramidas. 2015. Zolpidem and eszopiclone prime α1β2γ2 GABAA receptors for longer duration of activity. *Br. J. Pharmacol.* 172:3522–3536. https://doi.org/10.1111/bph.13142

Dworak, M., R.W. McCarley, T. Kim, A.V. Kalinchuk, and R. Basheer. 2010. Sleep and brain energy levels: ATP changes during sleep. *J. Neurosci.* 30: 9007–9016. https://doi.org/10.1523/JNEUROSCI.1423-10.2010

Elmore, M.R.P., A.R. Najafi, M.A. Koike, N.N. Dagher, E.E. Spangenberg, R.A. Rice, M. Kitazawa, B. Matusow, H. Nguyen, B.L. West, and K.N. Green. 2014. Colony-stimulating factor 1 receptor signaling is necessary for microglia viability, unmasking a microglia progenitor cell in the adult brain. *Neuron*. 82:380–397. https://doi.org/10.1016/j.neuron.2014.02.040

Fang, J., Y. Wang, and J.M. Krueger. 1997. Mice lacking the TNF 55 kDa receptor fail to sleep more after TNFalpha treatment. *J. Neurosci.* 17: 5949–5955. https://doi.org/10.1523/JNEUROSCI.17-15-05949.1997

Fattinger, S., T.T. de Beukelaar, K.L. Ruddy, C. Volk, N.C. Heyse, J.A. Herbst, R.H.R. Hahnloser, N. Wenderoth, and R. Huber. 2017. Deep sleep maintains learning efficiency of the human brain. *Nat. Commun.* 8: 15405. https://doi.org/10.1038/ncomms15405

Favuzzi, E., S. Huang, G.A. Saldi, L. Binan, L.A. Ibrahim, M. Fernández-Otero, Y. Cao, A. Zeine, A. Sefah, K. Zheng, et al. 2021. GABA-receptive microglia selectively sculpt developing inhibitory circuits. *Cell*. 184: 4048–4063.e32. https://doi.org/10.1016/j.cell.2021.06.018

Fonken, L.K., M.G. Frank, M.M. Kitt, R.M. Barrientos, L.R. Watkins, and S.F. Maier. 2015. Microglia inflammatory responses are controlled by an intrinsic circadian clock. *Brain Behav. Immun.* 45:171–179. https://doi.org/10.1016/j.bbi.2014.11.009

Franklin, K.B., and G. Paxinos. 2008. The Mouse Brain in Stereotaxic Coordinates, Compact. Third edition. Elsevier, Amsterdam, Netherlands.

Funk, C.M., K. Peelman, M. Bellesi, W. Marshall, C. Cirelli, and G. Tononi. 2017. Role of somatostatin-positive cortical interneurons in the generation of sleep slow waves. *J. Neurosci.* 37:9132–9148. https://doi.org/10.1523/JNEUROSCI.1303-17.2017

Garré, J.M., H.M. Silva, J.J. Lafaille, and G. Yang. 2017. CX3CR1+ monocytes modulate learning and learning-dependent dendritic spine remodeling via TNF-α. *Nat. Med.* 23:714–722. https://doi.org/10.1038/nm.4340

Goldmann, T., P. Wieghofer, P.F. Müller, Y. Wolf, D. Varol, S. Yona, S.M. Brendecke, K. Kierdorf, O. Staszewski, M. Datta, et al. 2013. A new type of microglia gene targeting shows TAK1 to be pivotal in CNS autoimmune inflammation. *Nat. Neurosci.* 16:1618–1626. https://doi.org/10.1038/nn.3531

Grivennikov, S.I., A.V. Tumanov, D.J. Liepinsh, A.A. Kruglov, B.I. Marakusha, A.N. Shakhov, T. Murakami, L.N. Drutskaya, I. Förster, B.E. Clausen, et al. 2005. Distinct and nonredundant in vivo functions of TNF produced by t cells and macrophages/neutrophils: Protective and deleterious effects. *Immunity*. 22:93–104. https://doi.org/10.1016/j.immuni.2004.11.016

Hanlon, E.C., U. Faraguna, V.V. Vyazovskiy, G. Tononi, and C. Cirelli. 2009. Effects of skilled training on sleep slow wave activity and cortical gene expression in the rat. *Sleep*. 32:719–729. https://doi.org/10.1093/sleep/32.6.719

Hay, Y.A., N. Deperrois, T. Fuchsberger, T.M. Quarrell, A.-L. Koerling, and O. Paulsen. 2021. Thalamus mediates neocortical down state transition via $GABA_B$-receptor-targeting interneurons. *Neuron*. 109:2682–2690.e5. https://doi.org/10.1016/j.neuron.2021.06.030

Henderson, F., V. Vialou, S. El Mestikawy, and V. Fabre. 2017. Effects of social defeat stress on sleep in mice. *Front. Behav. Neurosci.* 11:227. https://doi.org/10.3389/fnbeh.2017.00227

Hill, R.A., J. Medved, K.D. Patel, and A. Nishiyama. 2014. Organotypic slice cultures to study oligodendrocyte dynamics and myelination. *J. Vis. Exp.* 90:e51835. https://doi.org/10.3791/51835

Hoffmann, K., Y. Baqi, M.S. Morena, M. Glänzel, C.E. Müller, and I. von Kügelgen. 2009. Interaction of new, very potent non-nucleotide antagonists with Arg256 of the human platelet P2Y12 receptor. *J. Pharmacol. Exp. Ther.* 331:648–655. https://doi.org/10.1124/jpet.109.156687

Holbrook, J., S. Lara-Reyna, H. Jarosz-Griffiths, and M. McDermott. 2019. Tumour necrosis factor signalling in health and disease. *F1000Res.* 8: F1000 Faculty Rev-111. https://doi.org/10.12688/f1000research.17023.1

Hubbard, J., T.C. Gent, M.M.B. Hoekstra, Y. Emmenegger, V. Mongrain, H.-P. Landolt, A.R. Adamantidis, and P. Franken. 2020. Rapid fast-delta decay following prolonged wakefulness marks a phase of wake-inertia in NREM sleep. *Nat. Commun.* 11:3130. https://doi.org/10.1038/s41467-020-16915-0

Huber, R., M.F. Ghilardi, M. Massimini, and G. Tononi. 2004. Local sleep and learning. *Nature*. 430:78–81. https://doi.org/10.1038/nature02663

Irwin, M.R. 2019. Sleep and inflammation: Partners in sickness and in health. *Nat. Rev. Immunol.* 19:702–715. https://doi.org/10.1038/s41577-019-0190-z

Jung, S., J. Aliberti, P. Graemmel, M.J. Sunshine, G.W. Kreutzberg, A. Sher, and D.R. Littman. 2000. Analysis of fractalkine receptor CX(3)CR1 function by targeted deletion and green fluorescent protein reporter gene insertion. *Mol. Cell. Biol.* 20:4106–4114. https://doi.org/10.1128/MCB.20.11.4106-4114.2000

Kettenmann, H., F. Kirchhoff, and A. Verkhratsky. 2013. Microglia: New roles for the synaptic stripper. *Neuron*. 77:10–18. https://doi.org/10.1016/j.neuron.2012.12.023

Klinzing, J.G., N. Niethard, and J. Born. 2019. Mechanisms of systems memory consolidation during sleep. *Nat. Neurosci.* 22:1598–1610. https://doi.org/10.1038/s41593-019-0467-3

Krueger, J.M., P. Taishi, A. De, C.J. Davis, B.D. Winters, J. Clinton, E. Szentirmai, and M.R. Zielinski. 2010. ATP and the purine type 2 X7 receptor affect sleep. *J. Appl. Physiol.* 109:1318–1327. https://doi.org/10.1152/japplphysiol.00586.2010

Lagache, T., A. Grassart, S. Dallongeville, O. Faklaris, N. Sauvonnet, A. Dufour, L. Danglot, and J.-C. Olivo-Marin. 2018. Mapping molecular assemblies with fluorescence microscopy and object-based spatial statistics. *Nat. Commun.* 9:698. https://doi.org/10.1038/s41467-018-03053-x

Lee, J.K., and M.G. Tansey. 2013. Microglia isolation from adult mouse brain. *Methods Mol. Biol.* 1041:17–23. https://doi.org/10.1007/978-1-62703-520-0_3

Lee, H.-K., K. Kameyama, R.L. Huganir, and M.F. Bear. 1998. NMDA induces long-term synaptic depression and dephosphorylation of the GluR1 subunit of AMPA receptors in hippocampus. *Neuron.* 21:1151–1162. https://doi.org/10.1016/S0896-6273(00)80632-7

Lemieux, M., S. Chauvette, and I. Timofeev. 2015. Neocortical inhibitory activities and long-range afferents contribute to the synchronous onset of silent states of the neocortical slow oscillation. *J. Neurophysiol.* 113:768–779. https://doi.org/10.1152/jn.00858.2013

Lewitus, G.M., S.C. Konefal, A.D. Greenhalgh, H. Pribiag, K. Augereau, and D. Stellwagen. 2016. Microglial TNF-α suppresses cocaine-induced plasticity and behavioral sensitization. *Neuron.* 90:483–491. https://doi.org/10.1016/j.neuron.2016.03.030

Li, Y., X.F. Du, C.S. Liu, Z.L. Wen, and J.L. Du. 2012. Reciprocal regulation between resting microglial dynamics and neuronal activity in vivo. *Dev. Cell.* 23:1189–1202. https://doi.org/10.1016/j.devcel.2012.10.027

Li, W., L. Ma, G. Yang, and W.-B. Gan. 2017. REM sleep selectively prunes and maintains new synapses in development and learning. *Nat. Neurosci.* 20:427–437. https://doi.org/10.1038/nn.4479

Liu, Y.U., Y. Ying, Y. Li, U.B. Eyo, T. Chen, J. Zheng, A.D. Umpierre, J. Zhu, D.B. Bosco, H. Dong, and L.-J. Wu. 2019. Neuronal network activity controls microglial process surveillance in awake mice via norepinephrine signaling. *Nat. Neurosci.* 22:1771–1781. https://doi.org/10.1038/s41593-019-0511-3

Liu, H., X. Wang, L. Chen, L. Chen, S.E. Tsirka, S. Ge, and Q. Xiong. 2021. Microglia modulate stable wakefulness via the thalamic reticular nucleus in mice. *Nat. Commun.* 12:4646. https://doi.org/10.1038/s41467-021-24915-x

Madisen, L., T.A. Zwingman, S.M. Sunkin, S.W. Oh, H.A. Zariwala, H. Gu, L.L. Ng, R.D. Palmiter, M.J. Hawrylycz, A.R. Jones, et al. 2010. A robust and high-throughput Cre reporting and characterization system for the whole mouse brain. *Nat. Neurosci.* 13:133–140. https://doi.org/10.1038/nn.2467

Madry, C., and D. Attwell. 2015. Receptors, ion channels, and signaling mechanisms underlying microglial dynamics. *J. Biol. Chem.* 290:12443–12450. https://doi.org/10.1074/jbc.R115.637157

Madry, C., I.L. Arancibia-Cárcamo, V. Kyrargyri, V.T.T. Chan, N.B. Hamilton, and D. Attwell. 2018. Effects of the ecto-ATPase apyrase on microglial ramification and surveillance reflect cell depolarization, not ATP depletion. *Proc. Natl. Acad. Sci. USA.* 115:E1608–E1617. https://doi.org/10.1073/pnas.1715354115

Marsden, K.C., A. Shemesh, K.U. Bayer, and R.C. Carroll. 2010. Selective translocation of Ca^{2+}/calmodulin protein kinase IIalpha (CaMKIIalpha) to inhibitory synapses. *Proc. Natl. Acad. Sci. USA.* 107:20559–20564. https://doi.org/10.1073/pnas.1010346107

Marshall, L., H. Helgadóttir, M. Mölle, and J. Born. 2006. Boosting slow oscillations during sleep potentiates memory. *Nature.* 444:610–613. https://doi.org/10.1038/nature05278

Miyamoto, A., H. Wake, A.W. Ishikawa, K. Eto, K. Shibata, H. Murakoshi, S. Koizumi, A.J. Moorhouse, Y. Yoshimura, and J. Nabekura. 2016a. Microglia contact induces synapse formation in developing somatosensory cortex. *Nat. Commun.* 7:12540. https://doi.org/10.1038/ncomms12540

Miyamoto, D., D. Hirai, C.C.A. Fung, A. Inutsuka, M. Odagawa, T. Suzuki, R. Boehringer, C. Adaikkan, C. Matsubara, N. Matsuki, et al. 2016b. Top-down cortical input during NREM sleep consolidates perceptual memory. *Science.* 352:1315–1318. https://doi.org/10.1126/science.aaf0902

Nagai, H., L. de Vivo, M. Bellesi, M.F. Ghilardi, G. Tononi, and C. Cirelli. 2017. Sleep consolidates motor learning of complex movement sequences in mice. *Sleep.* 40:zsw059. https://doi.org/10.1093/sleep/zsw059

Nguyen, P.T., L.C. Dorman, S. Pan, I.D. Vainchtein, R.T. Han, H. Nakao-Inoue, S.E. Taloma, J.J. Barron, A.B. Molofsky, M.A. Kheirbek, and A.V. Molofsky. 2020. Microglial remodeling of the extracellular matrix promotes synapse plasticity. *Cell.* 182:388–403.e15. https://doi.org/10.1016/j.cell.2020.05.050

Niethard, N., H.-V.V. Ngo, I. Ehrlich, and J. Born. 2018. Cortical circuit activity underlying sleep slow oscillations and spindles. *Proc. Natl. Acad. Sci. USA.* 115:E9220–E9229. https://doi.org/10.1073/pnas.1805517115

Nir, Y., R.J. Staba, T. Andrillon, V.V. Vyazovskiy, C. Cirelli, I. Fried, and G. Tononi. 2011. Regional Slow Waves and Spindles in Human Sleep. *Neuron.* 70:153–169. https://doi.org/10.1016/j.neuron.2011.02.043

Noya, S.B., D. Colameo, F. Brüning, A. Spinnler, D. Mircsof, L. Opitz, M. Mann, S.K. Tyagarajan, M.S. Robles, and S.A. Brown. 2019. The forebrain synaptic transcriptome is organized by clocks but its proteome is driven by sleep. *Science.* 366:eaav2642. https://doi.org/10.1126/science.aav2642

Olivo-Marin, J.-C. 2002. Extraction of spots in biological images using multiscale products. *Pattern Recognit.* 35:1989–1996. https://doi.org/10.1016/S0031-3203(01)00127-3

Parkhurst, C.N., G. Yang, I. Ninan, J.N. Savas, J.R. Yates III, J.J. Lafaille, B.L. Hempstead, D.R. Littman, and W.-B. Gan. 2013. Microglia promote learning-dependent synapse formation through brain-derived neurotrophic factor. *Cell.* 155:1596–1609. https://doi.org/10.1016/j.cell.2013.11.030

Pascual, O., S. Ben Achour, P. Rostaing, A. Triller, and A. Bessis. 2012. Microglia activation triggers astrocyte-mediated modulation of excitatory neurotransmission. *Proc. Natl. Acad. Sci. USA.* 109:E197–E205. https://doi.org/10.1073/pnas.1111098109

Petrini, E.M., T. Ravasenga, T.J. Hausrat, G. Iurilli, U. Olcese, V. Racine, J.-B. Sibarita, T.C. Jacob, S.J. Moss, F. Benfenati, et al. 2014. Synaptic recruitment of gephyrin regulates surface GABAA receptor dynamics for the expression of inhibitory LTP. *Nat. Commun.* 5:3921. https://doi.org/10.1038/ncomms4921

Pinto, M.J., L. Cottin, F. Dingli, V. Laigle, L.F. Ribeiro, A. Triller, F. Henderson, D. Loew, V. Fabre, and A. Bessis. 2023. Microglial TNFα orchestrates protein phosphorylation in the cortex during the sleep period and controls homeostatic sleep. *EMBO J.* 42:e111485. https://doi.org/10.15252/embj.2022111485

Porkka-Heiskanen, T. 2013. Sleep homeostasis. *Curr. Opin. Neurobiol.* 23:799–805. https://doi.org/10.1016/j.conb.2013.02.010

Rockstrom, M.D., L. Chen, P. Taishi, J.T. Nguyen, C.M. Gibbons, S.C. Veasey, and J.M. Krueger. 2018. Tumor necrosis factor alpha in sleep regulation. *Sleep Med. Rev.* 40:69–78. https://doi.org/10.1016/j.smrv.2017.10.005

Rogers, J.T., J.M. Morganti, A.D. Bachstetter, C.E. Hudson, M.M. Peters, B.A. Grimmig, E.J. Weeber, P.C. Bickford, and C. Gemma. 2011. CX3CR1 deficiency leads to impairment of hippocampal cognitive function and synaptic plasticity. *J. Neurosci.* 31:16241–16250. https://doi.org/10.1523/JNEUROSCI.3667-11.2011

Rolls, A., D. Colas, A. Adamantidis, M. Carter, T. Lanre-Amos, H.C. Heller, and L. de Lecea. 2011. Optogenetic disruption of sleep continuity impairs memory consolidation. *Proc. Natl. Acad. Sci. USA.* 108:13305–13310. https://doi.org/10.1073/pnas.1015633108

Santello, M., P. Bezzi, and A. Volterra. 2011. TNFα controls glutamatergic gliotransmission in the hippocampal dentate gyrus. *Neuron.* 69:988–1001. https://doi.org/10.1016/j.neuron.2011.02.003

Schafer, D.P., E.K. Lehrman, A.G. Kautzman, R. Koyama, A.R. Mardinly, R. Yamasaki, R.M. Ransohoff, M.E. Greenberg, B.A. Barres, and B. Stevens. 2012. Microglia sculpt postnatal neural circuits in an activity and complement-dependent manner. *Neuron.* 74:691–705. https://doi.org/10.1016/j.neuron.2012.03.026

Schuman, B., S. Dellal, A. Prönneke, R. Machold, and B. Rudy. 2021. Neocortical layer 1: An elegant solution to top-down and bottom-up integration. *Annu. Rev. Neurosci.* 44:221–252. https://doi.org/10.1146/annurev-neuro-100520-012117

Shoham, S., D. Davenne, A.B. Cady, C.A. Dinarello, and J.M. Krueger. 1987. Recombinant tumor necrosis factor and interleukin 1 enhance slow-wave sleep. *Am. J. Physiol.* 253:R142–R149. https://doi.org/10.1152/ajpregu.1987.253.1.R142

Solle, M., J. Labasi, D.G. Perregaux, E. Stam, N. Petrushova, B.H. Koller, R.J. Griffiths, and C.A. Gabel. 2001. Altered cytokine production in mice lacking P2X(7) receptors. *J. Biol. Chem.* 276:125–132. https://doi.org/10.1074/jbc.M006781200

Stellwagen, D., and R.C. Malenka. 2006. Synaptic scaling mediated by glial TNF-alpha. *Nature.* 440:1054–1059. https://doi.org/10.1038/nature04671

Stogsdill, J.A., K. Kim, L. Binan, S.L. Farhi, J.Z. Levin, and P. Arlotta. 2022. Pyramidal neuron subtype diversity governs microglia states in the neocortex. *Nature.* 608:750–756. https://doi.org/10.1038/s41586-022-05056-7

Stowell, R.D., G.O. Sipe, R.P. Dawes, H.N. Batchelor, K.A. Lordy, B.S. Whitelaw, M.B. Stoessel, J.M. Bidlack, E. Brown, M. Sur, and A.K. Majewska. 2019. Noradrenergic signaling in the wakeful state inhibits microglial

surveillance and synaptic plasticity in the mouse visual cortex. *Nat. Neurosci.* 22:1782–1792. https://doi.org/10.1038/s41593-019-0514-0

Surprenant, A., F. Rassendren, E. Kawashima, R.A. North, and G. Buell. 1996. The cytolytic P2Z receptor for extracellular ATP identified as a P2X receptor (P2X7). *Science.* 272:735–738. https://doi.org/10.1126/science.272.5262.735

Suzuki, T., I. Hide, K. Ido, S. Kohsaka, K. Inoue, and Y. Nakata. 2004. Production and release of neuroprotective tumor necrosis factor by P2X7 receptor-activated microglia. *J. Neurosci.* 24:1–7. https://doi.org/10.1523/JNEUROSCI.3792-03.2004

Szabó, Z., L. Héja, G. Szalay, O. Kékesi, A. Füredi, K. Szebényi, Á. Dobolyi, T.I. Orbán, O. Kolacsek, T. Tompa, et al. 2017. Extensive astrocyte synchronization advances neuronal coupling in slow wave activity in vivo. *Sci. Rep.* 7:6018. https://doi.org/10.1038/s41598-017-06073-7

Szentirmai, É., and L. Kapás. 2019. Sleep and body temperature in TNFα knockout mice: The effects of sleep deprivation, β3-AR stimulation and exogenous TNFα. *Brain Behav. Immun.* 81:260–271. https://doi.org/10.1016/j.bbi.2019.06.022

Taniguchi, H., M. He, P. Wu, S. Kim, R. Paik, K. Sugino, D. Kvitsiani, Y. Fu, J. Lu, Y. Lin, et al. 2011. A resource of Cre driver lines for genetic targeting of GABAergic neurons in cerebral cortex. *Neuron.* 71:995–1013. https://doi.org/10.1016/j.neuron.2011.07.026

Thion, M.S., F. Ginhoux, and S. Garel. 2018. Microglia and early brain development: An intimate journey. *Science.* 362:185–189. https://doi.org/10.1126/science.aat0474

Tononi, G., and C. Cirelli. 2019. Sleep and synaptic down-selection. *Eur. J. Neurosci.* 51:413–421. https://doi.org/10.1111/ejn.14335

Tremblay, R., S. Lee, and B. Rudy. 2016. GABAergic interneurons in the neocortex: From cellular properties to circuits. *Neuron.* 91:260–292. https://doi.org/10.1016/j.neuron.2016.06.033

Vaidyanathan, T.V., M. Collard, S. Yokoyama, M.E. Reitman, and K.E. Poskanzer. 2021. Cortical astrocytes independently regulate sleep depth and duration via separate GPCR pathways. *Elife.* 10:e63329. https://doi.org/10.7554/eLife.63329

Vyazovskiy, V.V., G. Ruijgrok, T. Deboer, and I. Tobler. 2006. Running wheel accessibility affects the regional electroencephalogram during sleep in mice. *Cereb. Cortex.* 16:328–336. https://doi.org/10.1093/cercor/bhi110

Vyazovskiy, V.V., B.A. Riedner, C. Cirelli, and G. Tononi. 2007. Sleep homeostasis and cortical synchronization: II. A local field potential study of sleep slow waves in the rat. *Sleep.* 30:1631–1642. https://doi.org/10.1093/sleep/30.12.1631

Vyazovskiy, V.V., C. Cirelli, M. Pfister-Genskow, U. Faraguna, and G. Tononi. 2008. Molecular and electrophysiological evidence for net synaptic potentiation in wake and depression in sleep. *Nat. Neurosci.* 11:200–208. https://doi.org/10.1038/nn2035

Wang, C., H. Yue, Z. Hu, Y. Shen, J. Ma, J. Li, X.-D. Wang, L. Wang, B. Sun, P. Shi, et al. 2020. Microglia mediate forgetting via complement-dependent synaptic elimination. *Science.* 367:688–694. https://doi.org/10.1126/science.aaz2288

Weinhard, L., G. di Bartolomei, G. Bolasco, P. Machado, N.L. Schieber, U. Neniskyte, M. Exiga, A. Vadisiute, A. Raggioli, A. Schertel, et al. 2018. Microglia remodel synapses by presynaptic trogocytosis and spine head filopodia induction. *Nat. Commun.* 9:1228. https://doi.org/10.1038/s41467-018-03566-5

Yang, G., C.S.W. Lai, J. Cichon, L. Ma, W. Li, and W.-B. Gan. 2014. Sleep promotes branch-specific formation of dendritic spines after learning. *Science.* 344:1173–1178. https://doi.org/10.1126/science.1249098

Yona, S., K.-W. Kim, Y. Wolf, A. Mildner, D. Varol, M. Breker, D. Strauss-Ayali, S. Viukov, M. Guilliams, A. Misharin, et al. 2013. Fate mapping reveals origins and dynamics of monocytes and tissue macrophages under homeostasis. *Immunity.* 38:79–91. https://doi.org/10.1016/j.immuni.2012.12.001

Yoshida, H., Z. Peterfi, F. García-García, R. Kirkpatrick, T. Yasuda, and J.M. Krueger. 2004. State-specific asymmetries in EEG slow wave activity induced by local application of TNFalpha. *Brain Res.* 1009:129–136. https://doi.org/10.1016/j.brainres.2004.02.055

Zamanian, J.L., L. Xu, L.C. Foo, N. Nouri, L. Zhou, R.G. Giffard, and B.A. Barres. 2012. Genomic analysis of reactive astrogliosis. *J. Neurosci.* 32:6391–6410. https://doi.org/10.1523/JNEUROSCI.6221-11.2012

Zeisel, A., H. Hochgerner, P. Lönnerberg, A. Johnsson, F. Memic, J. van der Zwan, M. Häring, E. Braun, L.E. Borm, G. La Manno, et al. 2018. Molecular architecture of the mouse nervous system. *Cell.* 174:999–1014.e22. https://doi.org/10.1016/j.cell.2018.06.021

Zielinski, M.R., D.N. Atochin, J.M. McNally, J.T. McKenna, P.L. Huang, R.E. Strecker, and D. Gerashchenko. 2019. Somatostatin+/nNOS+ neurons are involved in delta electroencephalogram activity and cortical-dependent recognition memory. *Sleep.* 42:zsz143. https://doi.org/10.1093/sleep/zsz143

Zucca, S., G. D'Urso, V. Pasquale, D. Vecchia, G. Pica, S. Bovetti, C. Moretti, S. Varani, M. Molano-Mazón, M. Chiappalone, et al. 2017. An inhibitory gate for state transition in cortex. *Elife.* 6:e26177. https://doi.org/10.7554/eLife.26177

Supplemental material

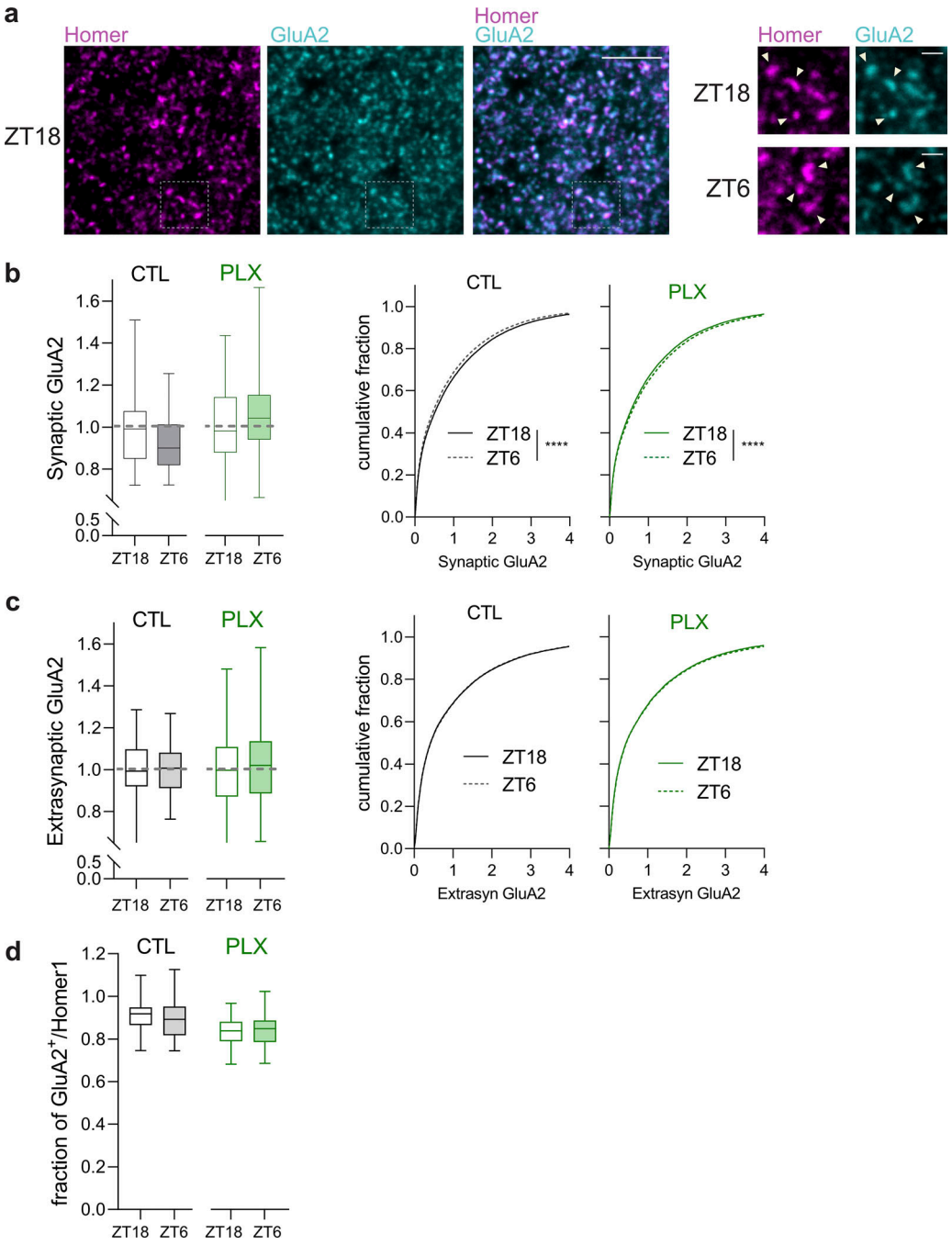

Figure S1. **AMPARs plasticity across the light/dark cycle. (a)** Confocal images showing downregulation of GluA2 (cyan) at Homer1⁺ clusters (magenta, arrowheads) at ZT6 in cortical L1. Scale bars, 5 and 1 µm. **(b)** Left: Mean intensity of GluA2 clusters at Homer1⁺ clusters. No statistical significance by nested two-tailed *t* test. Right: Cumulative fraction of GluA2 clusters' intensities at Homer1⁺ clusters in control CTL (black) and PLX3397 treated (green) mice. ****P < 0.0001, Kolmogorov–Smirnoff test. **(c)** Left: Mean intensity of GluA2 at extrasynaptic sites. No statistical significance by nested two-tailed *t* test. Right: Cumulative fraction of GluA2 clusters' intensities at extrasynaptic sites in controls CTL (black) and PLX3397 treated (green) mice. No statistical significance by Kolmogorov–Smirnoff test. **(d)** Fraction of Homer1⁺ clusters colocalized with GluA2 in controls CTL (black) and PLX3397 treated (green) mice. No statistical significance by nested two-tailed *t* test. **(b–d)** *n* = 46-58 FOVs from four to five mice per group. Results are presented as minimum to maximum box plots and cumulative distributions.

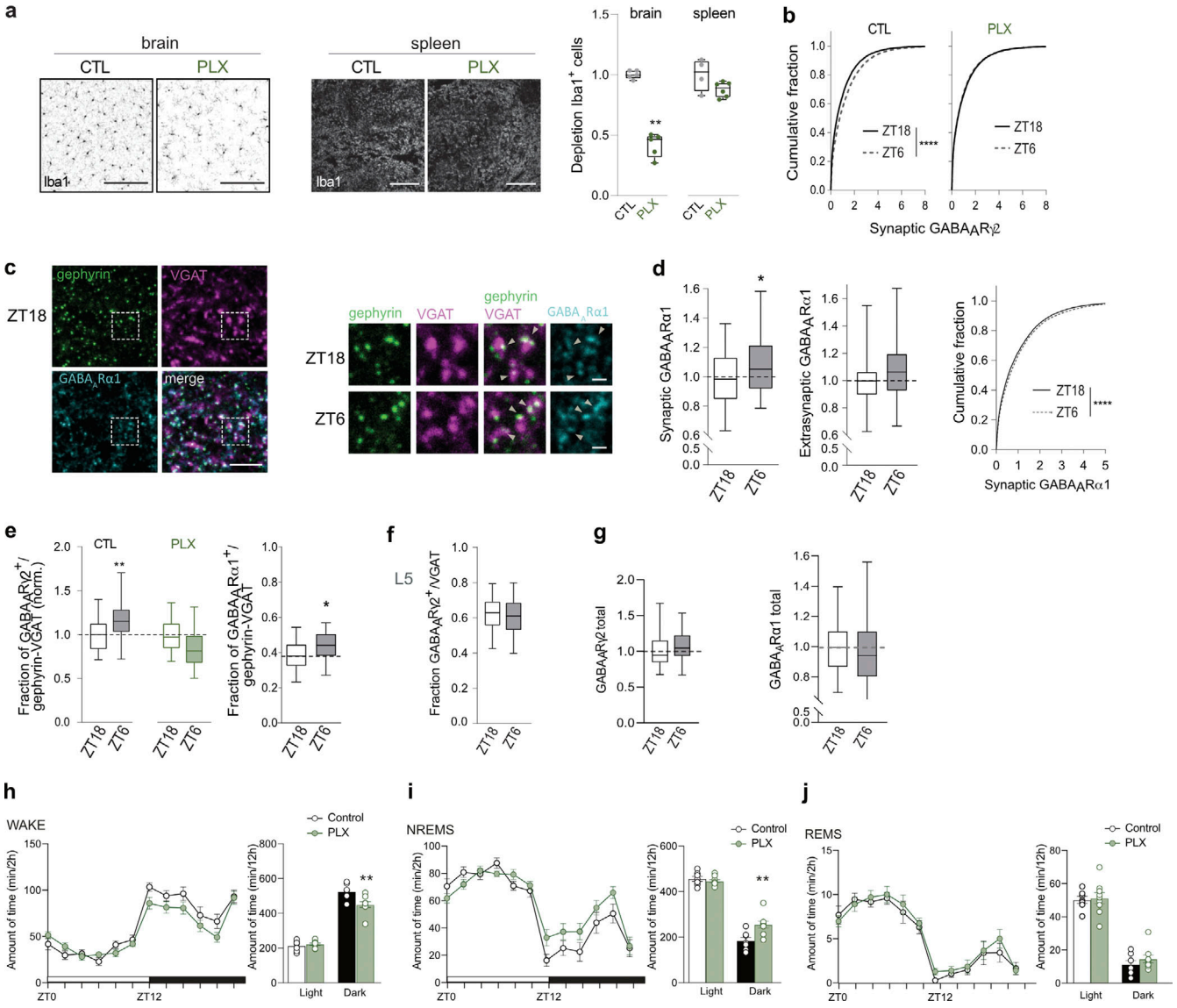

Figure S2. **GABA$_A$Rs plasticity across the light/dark cycle. (a)** Left: Confocal images of Iba1$^+$ cells revealing partial depletion in the brain, but not in the spleen, by 2-wk feeding with PLX3397-containing food (PLX). Scale bars, 200 µm. Right: Density of Iba1$^+$ cells normalized to CTL. *n* = 5 mice for CTL and PLX. **P < 0.01, unpaired two-tailed Mann–Whitney test. Data are mean ± SEM. **(b)** Left: Cumulative fraction of GABA$_A$Rγ2 clusters' intensities at gephyrin$^+$VGAT$^+$ synapses in cortical L1. ****P < 0.0001, Kolmogorov–Smirnoff. **(c)** Representative confocal images showing increase of GABA$_A$Rα1 (cyan) at cortical L1 inhibitory synapses (arrowhead: gephyrin$^+$VGAT$^+$) at ZT6 in comparison to ZT18. Scale bars, 5 and 1 µm. Dashed box corresponds to enlarged detail in ZT18. **(d)** Left: Mean intensity of GABA$_A$Rα1 clusters at gephyrin$^+$VGAT$^+$ synapses (synaptic) and at extrasynaptic sites. *P < 0.05, nested two-tailed *t* test. Right: Cumulative fraction of GABA$_A$Rα1 clusters' intensities at gephyrin$^+$VGAT$^+$ synapses. ****P < 0.0001, Kolmogorov–Smirnoff test. **(e)** Fraction of gephyrin$^+$VGAT$^+$ synapses colocalized to GABA$_A$Rs clusters. *P < 0.05 and **P < 0.01, nested two-tailed *t* test. **(f)** Fraction of somatic VGAT$^+$ cluster colocalized to GABA$_A$Rγ2 clusters in cortical L5. No statistical significance by nested two-tailed *t* test. **(g)** Mean intensity of total GABA$_A$Rγ2 (left) and GABA$_A$Rα1 signal (right). No statistical significance by nested two-tailed *t* test. **(b–g)** *n* = 53-60 FOVs from 5 mice per group. Results are presented as minimum to maximum box plots. **(h–j)** Amounts of vigilance states over 24 h in controls CTL (black) and PLX3397 treated (green) mice in Wake (h), NREMS (i), and REMS (j). Left panels: Amounts were reported by 2 h segments. Two-way rANOVA; Wake: treatment, F(1,14) = 4.128, P = 0.062; time: F(4.253,59.54) = 46.97, P < 0.0001; interaction F(11,154) = 1.751, P = 0.067; NREMS, treatment, F(1,14) = 3.596, P = 0.079; time: F(11,154) = 15.32, P < 0.0001; interaction F(11,154) = 1.452, P = 0.155, REMS, treatment, F(1,14) = 1.578, P = 0.2296; time: F(3.267,45.73) = 22.47, P < 0.0001; interaction F(11,154) = 0.650, P = 0.7832. Right panels: amounts were reported by 12 h segments. Mann–Whitney tests, **P < 0.01 CTL versus PLX3397. CTL, seven mice; PLX3397 treated, nine mice. Data are represented as mean ± SEM. In agreement with previous work (Corsi et al., 2022; Liu et al., 2021) microglia depletion affects time in wake and NREM sleep only in the dark phase.

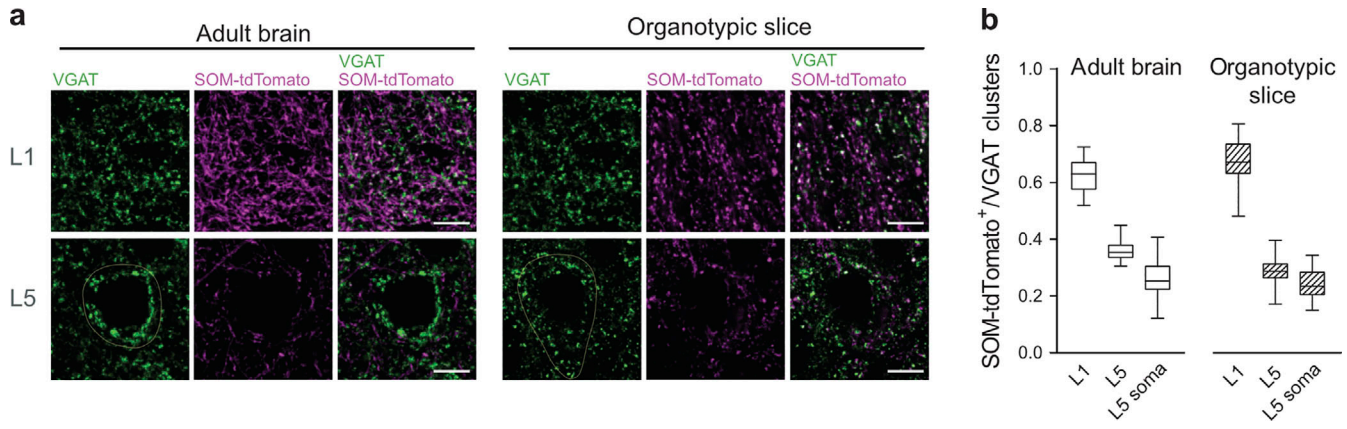

Figure S3. **SOM-IN⁺ inputs are distributed similarly in adult brain and organotypic slices. (a)** SOM-IN presynaptic boutons, identified in $SOM^{Cre/+}$:$R26^{tdTom/+}$ adult mice as SOM-tdTomato⁺VGAT⁺ terminals, are denser in upper cortical layers of brain and organotypic slices. Scale bars, 10 µm. **(b)** Fraction of VGAT⁺ puncta colocalized to SOM-tdTomato⁺ boutons. Of note, the majority of VGAT⁺ puncta in adult brain and organotypic slices cortical L1 are SOM-IN inputs. Adult brain: *n* = 31 (L1) and 33 (L5) FOVs from three $SOM^{Cre/+}$:$R26^{tdTom/+}$ mice. Organotypic slices: *n* = 24 (L1), 12 (L5) FOVs from 1 $SOM^{Cre/+}$:$R26^{tdTom/+}$ culture. Results are presented as minimum to maximum box plots.

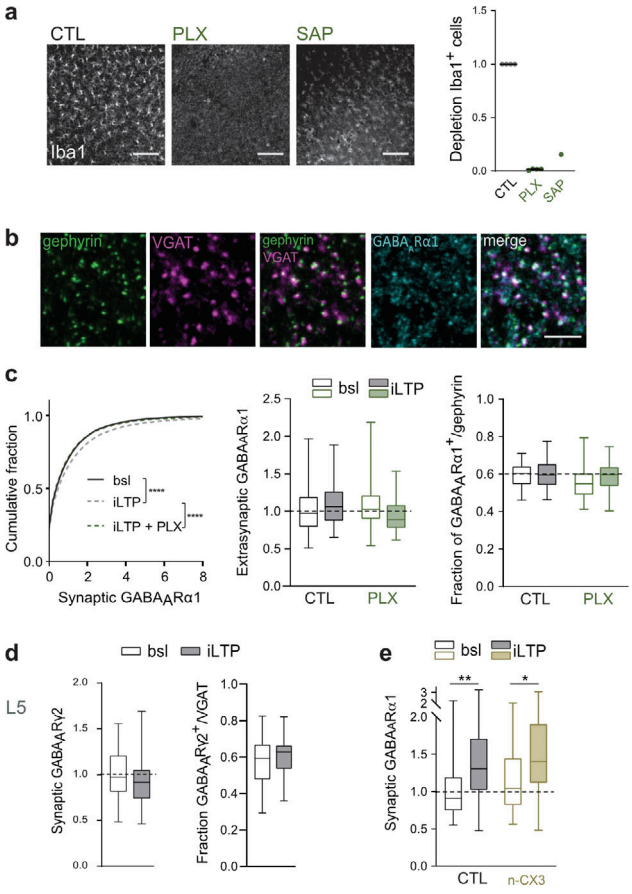

Figure S4. **Microglia are required for iLTP-induced $GABA_ARs$ plasticity. (a)** Left: Iba1⁺ cells are depleted in organotypic slices by PLX3397 (PLX) or Mac1-Saporin (SAP) treatment. Scale bars, 100 µm. Right: Density of Iba1⁺ cells normalized to untreated slices (CTL). *n* = 4 to 1 independent experiments. Data are mean ± SEM. Each datapoint represents one independent experiment. **(b)** Confocal images of inhibitory synaptic markers gephyrin, VGAT and $GABA_ARα1$ in organotypic slices cortical L1. Scale bar, 5 µm. **(c)** Left: Cumulative fraction of the intensity of $GABA_ARα1$ clusters at gephyrin⁺ cluster. ****P < 0,0001, Kolmogorov–Smirnoff. Middle: Mean intensity of extrasynaptic $GABA_ARα1$. Right: Fraction of gephyrin⁺ clusters colocalized to $GABA_ARα1$. No statistical significance by nested one-way ANOVA followed by Sidak's multiple comparison test. Results are presented as minimum to maximum box plots. *n* = 44 to 50 FOVs from six independent experiments. **(d)** Left: Mean intensity of $GABA_ARγ2$ clusters at VGAT⁺ clusters around NeuN⁺ cell bodies showing no changes in $GABA_ARγ2$ at putative somatic L5 synapses upon iLTP. Right: Fraction of VGAT⁺ clusters colocalized to $GABA_ARγ2$ cluster in putative L5. No statistical significance by nested two-tailed *t* test. *n* = 43 to 45 FOVs from six independent experiments. **(e)** Mean intensity of $GABA_ARα1$ clusters at gephyrin⁺ cluster showing no suppression of iLTP effect by CX3CL1 neutralizing antibody (n-CX3). *n* = 63 to 69 FOVs from six independent experiments. *P < 0.05 and **P < 0.01, nested one-way ANOVA followed by Sidak's multiple comparison test. **(d and e)** Results are presented as minimum to maximum box-plots.

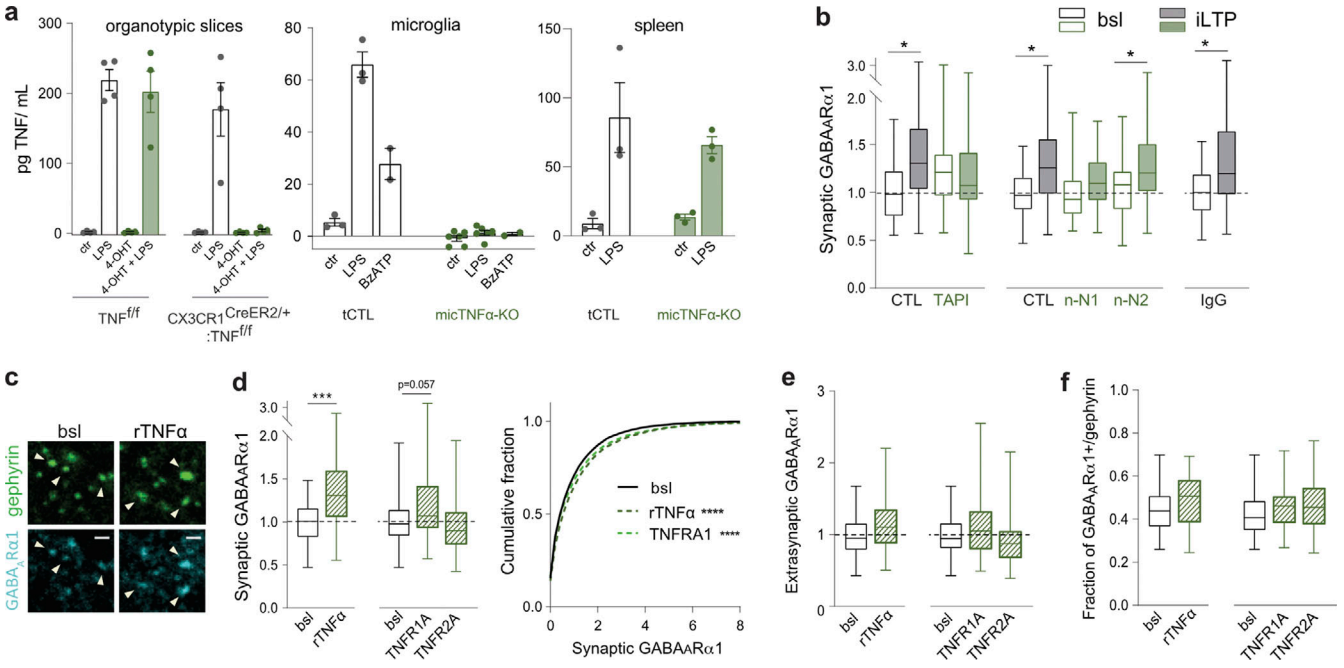

Figure S5. **TNFα controls GABA$_A$R plasticity. (a)** Conditional deletion of TNFα from CX3CR1-expressing cells in organotypic slices and in vivo assessed by ELISA. Graphs show TNFα concentration (pg/ml) as mean ± SEM. Left: Complete lack of LPS-induced TNFα production by organotypic slices upon 4-OHT-induced recombination of microglial TNFα in a CX3CR1$^{CreERT2/+}$:TNF$^{f/f}$ background but not control slices (TNF$^{f/f}$). *n* = 2 replicates from two individual experiments. Middle: Following feeding with tamoxifen-containing food, LPS- or BzATP-induced TNFα release by adult mouse primary microglia observed in transgenic controls (tCTL, CX3CR1$^{GFP/+}$:TNF$^{f/f}$) but not on microglia-TNFα depleted mice (micTNFα-KO, CX3CR1$^{CreERT2/+}$:TNF$^{f/f}$). *n* = two to six mice per group. Right: On spleen cultures from tamoxifen-treated mice, LPS-induced TNFα release is not affected in both tCTL and micTNF-KO, demonstrating microglia-specific TNFα deletion in vivo. *n* = 3 mice per condition. **(b)** Mean intensity of GABA$_A$Rα1 clusters at gephyrin$^+$ clusters upon blockade of TNFα cleavage (TAPI), neutralization of TNFR1 (n-N1), TNFR2 (n-N2), and control IgGs (IgG). *n* = 62 to 89 FOVs from five to nine independent experiments. *P < 0.05, nested one-way ANOVA followed by Sidak's multiple comparison test. **(c)** Representative images showing increase of GABA$_A$Rα1 (cyan) at gephyrin$^+$ clusters (arrowhead, green) after 20 min treatment with recombinant TNFα (rTNFα). Scale bars, 1 µm. **(d)** Effect of rTNFα and TNFR1 activating antibodies (TNFRA1), but not TNFR2 activating antibodies (TNFRA2), on GABA$_A$Rα1 at L1 synapses. Left: Mean intensity of GABA$_A$Rα1 clusters at gephyrin$^+$ clusters. ***P < 0.001, nested two-tailed *t* test (bsl compared to rTNFα); and no statistical significance by nested one-way ANOVA followed by Sidak's multiple comparison test (for bsl, TNFR1A and TNFR2A). Right: Cumulative fraction of the intensity of GABA$_A$Rα1 clusters at gephyrin$^+$ cluster. ****P < 0,0001, Kolmogorov–Smirnoff. **(e)** Mean intensity of GABA$_A$Rα1 clusters at extrasynaptic sites. **(f)** Fraction of gephyrin$^+$ clusters colocalized to GABA$_A$Rα1. **(e and f)** No statistical significance by nested two-tailed *t* test (bsl compared to rTNFα) and nested one-way ANOVA followed by Sidak's multiple comparison test (for bsl, TNFR1A, and TNFR2A). **(d–f)** *n* = 65 to 77 FOVs from eight independent experiments. **(b and d–f)** Results are presented as a minimum to maximum box plots.

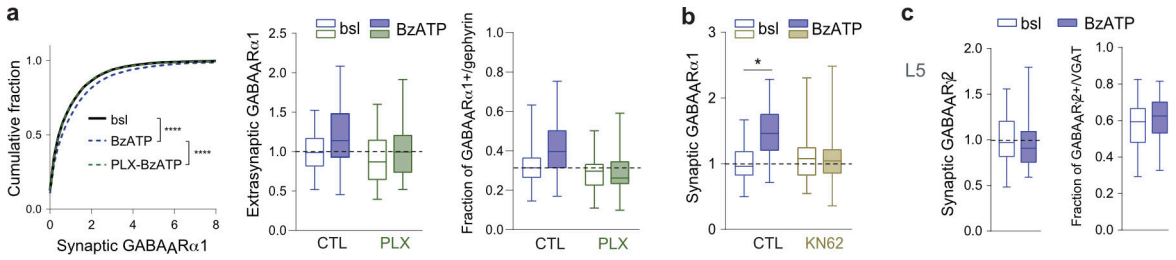

Figure S6. **BzATP-induced GABA$_A$R synaptic enrichment. (a)** Left: Cumulative fraction of GABA$_A$Rα1 clusters' intensities at gephyrin$^+$ cluster. ****P < 0,0001, Kolmogorov–Smirnoff test. Middle: Mean intensity of extrasynaptic GABA$_A$Rα1. Right: Fraction of gephyrin$^+$ clusters colocalized to GABA$_A$Rα1. No statistical significance by nested one-way ANOVA followed by Sidak's multiple comparison test. *n* = 49 to 63 FOVs from five independent experiments. **(b)** Mean intensity of GABA$_A$Rα1 clusters at gephyrin$^+$ cluster. KN62, a CaMKII inhibitor, abolishes BzATP-induced synaptic upregulation of GABA$_A$Rα1, indicative of a shared molecular mechanism at the neuronal level with iLTP. *n* = 53 to 57 FOVs from five independent experiments. *P < 0.05, nested one-way ANOVA followed by Sidak's multiple comparison test. **(c)** BzATP has no effect on synaptic GABA$_A$R at putative L5. Left: Mean intensity of GABA$_A$Rγ2 clusters at VGAT$^+$ clusters. Right: Fraction of VGAT$^+$ clusters colocalized to GABA$_A$Rγ2 cluster. No statistical significance by nested two-tailed *t* test. *n* = 42 to 45 FOVs from six independent experiments. **(a–c)** Results are presented as a minimum to maximum box plots.

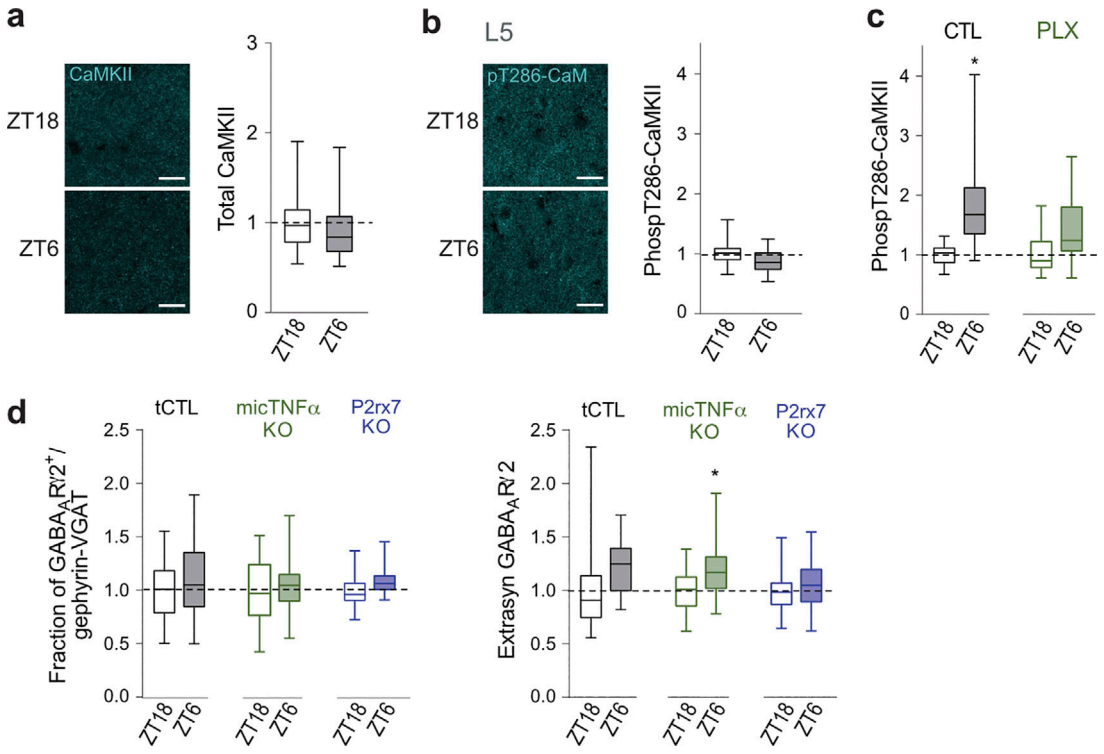

Figure S7. **Microglia control GABA$_A$R plasticity and fluctuations of CaMKII phosphorylation across the light/dark cycle. (a)** Left: Confocal images of L1 total CaMKII immunoreactivity showing no changes between ZT18 and ZT6 in transgenic control mice (tCTL). Scale bars, 20 µm. Right: Mean intensity of total CaMKII signal normalized to ZT18. No statistical significance by nested two-tailed *t* test. *n* = 40–50 FOVs from four to five mice per group. **(b)** Confocal images of L5 Thr286-phosphorylated CaMKII immunoreactivity. Scale bars, 20 µm. Right: Mean intensity of Thr286-phosphorylated CaMKII signal normalized to ZT18. No statistical significance by nested two-tailed *t* test. *n* = 32 to 40 FOVs from four to five mice per group. **(c)** Mean intensity of Thr286-phosphorylated CaMKII signal in L1 normalized to ZT18. *n* = 49 to 50 FOVs from 5 mice per group. *P < 0.05, nested two-tailed *t* test. **(d)** Left: Fraction of gephyrin$^+$VGAT$^+$ synapses colocalized to GABA$_A$R cluster. Right: Mean intensity of GABA$_A$R clusters at extrasynaptic sites. *n* = 48 to 65 FOVs from four to five mice per group. *P < 0.05, nested two-tailed *t* test. **(a–d)** Results are presented as minimum to maximum box-plots.

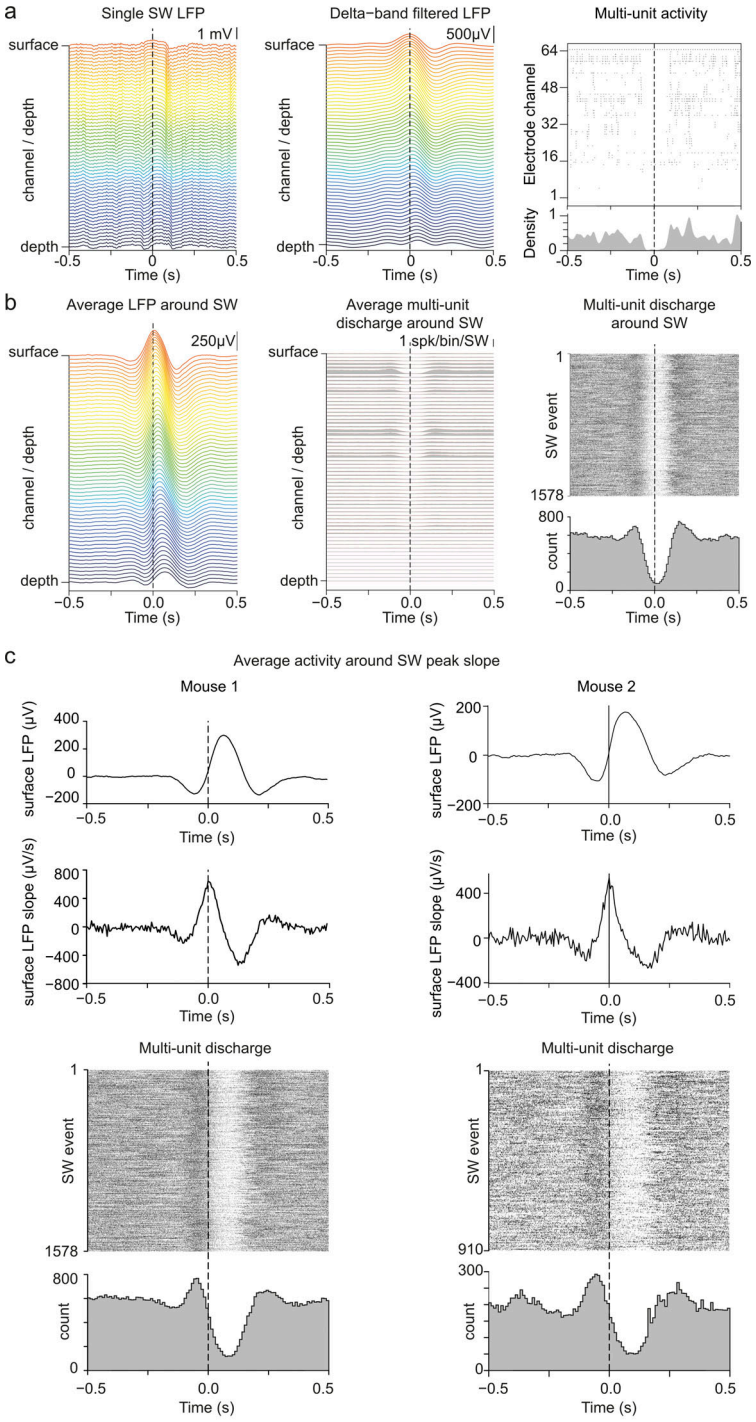

Figure S8. **SWs coincide with cortical down-states and peak upward slope corresponds to the onset of down-states. (a)** Example of single SW recorded across cortical layers by linear electrodes (with 20 µm spacing between the contacts). The channels are plotted and colored by depth. The top channel is located close to the surface, and the bottom channel ("depth") is located 1,275 µm below. Left: Raw local field potential (LFP) traces. Middle: Delta-band filtered LFP. Right: Multiunit activity across all electrode channels; each line corresponds to a channel, and each dot represents the time of an extracellular spike detected on the channel. The density of spikes detected on all channels is evaluated using a 10 ms Gaussian kernel and plotted at the bottom. **(b)** Average LFP and multi-unit activity around the peak of all SW detected in a 2 h-recording session. Left: Average LFP trace for each depth. Middle: Spike count around the peak of the SW; each line corresponds to the cross-correlogram between the times of the peak of SW and the multiunit activity of a single channel. Right: Rasters of the total multi-unit activity detected across all channels for each individual SW (each line corresponds to a SW event, each dot on this line to an extracellular spike); a grand histogram is indicated at the bottom. Note that there is a clear drop in the density of spikes around the peak of each SW indicating the correspondence between the SW and cortical down-states. **(c)** The peak upward slope corresponds to the drop of multiunit cortical activity below the basal firing rate. The results of two mice are displayed. Top: Average SW waveform at the surface centered on the time of maximal slope of the SW. Middle: Average derivative of the surface LFP around the time of maximal slope of the SW. Bottom: Raster and histogram of the multi-unit activity for all SWs, centered on the maximal slope of each SW.

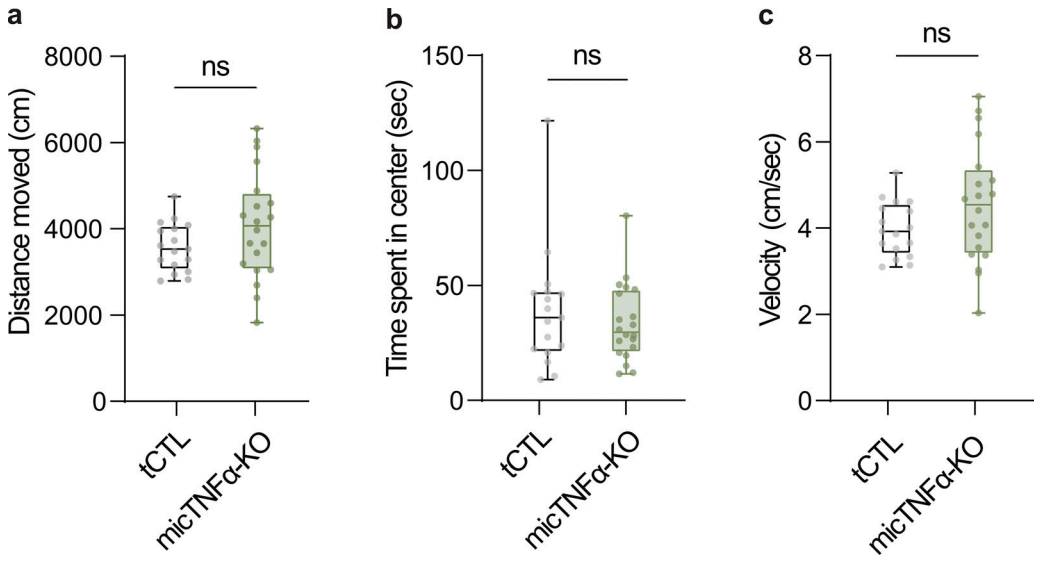

Figure S9. **Microglial TNFα does not modulate locomotor activity and anxiety-like behaviors. (a)** No significant differences were measured between tCTL and micTNFα-KO mice in the open-field test for the distance covered (two-tailed unpaired *t* test, t(35) = 1.533, P = 0.1324). **(b and c)** Time spent in the central zone (two-tailed unpaired *t* test, t(35) = 0.7278, P = 0.4716); and velocity (two-tailed unpaired *t* test, t(35) = 1.587, P = 0.1214). **(a–c)** *n* = 17 tCTL and 20 micTNFα-KO mice. Data are expressed as means ± SEM.

Provided online are Table S1, Table S2, Table S3, and Table S4. Table S1 shows sleep and wake characteristics in control and PLX3397 treated mice. Table S2 shows sleep and wake characteristics in control and micTNFα-KO mice. Table S3 is the list of the drugs and neutralizing or activating antibodies that were used in this study. Table S4 shows the list of antibodies and immunohistochemical methods used in this study.